

# **Simultaneous Effects of MHD and Porosity in Newtonian Nanofluid on Wavy Surface**



By

**Muhammad Awais**

**211-FBAS/MSMA/F14**

**Department of Mathematics and Statistics  
Faculty of Basic and Applied Sciences  
International Islamic University, Islamabad  
Pakistan**

**2016**





Accession No

TH-16772 <sup>US</sup>

MS  
620.106  
MUS

- 1. Navoflights
- 2. Head. Transmittal

# **Simultaneous Effects of MHD and Porosity in Newtonian Nanofluid on Wavy Surface**



By:

**Muhammad Awais**

Supervised by

**Dr. Rahmat Ellahi**

**Department of Mathematics and Statistics  
Faculty of Basic and Applied Sciences  
International Islamic University, Islamabad  
Pakistan**

**2016**

**Simultaneous Effects of MHD and Porosity in  
Newtonian Nanofluid on Wavy Surface**

By

**Muhammad Awais**

**A Thesis Submitted in the Partial Fulfillment  
of the Requirements for the Degree of**

**MASTER OF PHILOSOPHY IN  
MATHEMATICS**

Supervised by

**Dr. Rahmat Ellahi**

**Department of Mathematics and Statistics**

**Faculty of Basic and Applied Sciences**

**International Islamic University, Islamabad**

**Pakistan**

**2016**

# Certificate

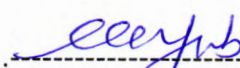
## Simultaneous Effects of MHD and Porosity in Newtonian Nanofluids on Wavy Surface


By

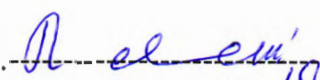
**Muhammad Awais**


A THESIS SUBMITTED IN PARTIAL FULFILLMENT OF  
THE REQUIREMENT FOR THE DEGREE OF MASTER OF PHILOSOPHY  
IN MATHEMATICS

**We accept this as conforming to the required standard**

1.   
Prof. Dr. Muhammad Ayub  
(External Examiner)

2.   
Dr. Ahmed Zeeshan  
(Internal Examiner)

3.   
Dr. Rahmat Ellahi  
(Supervisor)

4.   
Prof. Dr. Muhammad Arshad  
(Chairman)

**Department of Mathematics and Statistics**

**Faculty of Basic and Applied Sciences**

**International Islamic University, Islamabad**

**Pakistan**

**2016**

## Declaration

I hereby declare and affirm that this research work neither as whole nor as a part has been copied out from any source. It is further declare that I have developed this research work entirely on the basis of my personal efforts. If any part of this thesis is proven to be copied out or found to be a reproduction of some other, I shall stand by the consequences.

Moreover, no portion of the work presented in this thesis has been submitted in support of an application for other degree or qualification in this university or other institute of learning.

Signature:-\_\_\_\_\_

Muhammad Awais

Reg # 211-FBAS/MSMA/F14

# Dedication

*My beloved parents, grandmother (late), brothers*

*and*

*sisters*

# Acknowledgements

Primarily and foremost, I am thankful to Almighty Allah, who is the only creator and master of us, who created us from a clot and taught us to write with the pen who provided me the strength and ability to learn and achieve another milestone to a destination. Countless droods and slams upon prophet Muhammad (SAW) who is forever a torch of gaudiness, a source of knowledge and blessings for entire creation. His teachings shows us a way to live with dignity, stand with honor and learn to be humble.

Foremost thanks go to my supervisor **Dr. Rahmat Ellahi**, his dynamic supervision, guidance in a right direction, constant moral encouragements and motivation of hard work made my task easy and I completed my thesis well with in time. His comprehensive knowledge and logical way of thinking have been of greater value for me. His understanding, encouraging and personal guidance have provided a good basis to understand the field of fluid mechanics. His ideas and concepts have remarkable influence on my research skills. I have learned a lot from him.

I am much thankful to my senior fellow **Dr. Mohsin Hassan** for his valuable advice in discussions, his precious time to guide and gave his comments. I truthfully acknowledge his for the ideas he enthusiastically shared with me to produce my best work. He really helped me out in every problem.

I am grateful to **Dr. Muhammad Arshad**, Chairman Department of Mathematics for providing assess to facilities that ensured successful completion of my work.

A warm thanks to **Mr. Shafee, Mr. Muzammal Hameed Tariq, Mr. Ifraheem Waheed** and **Mr. Bilal Arain**, who offered me a lot of friendly help during my research work. Many thanks to **Dr. Ahmad Zeeshan** and **Dr. Mohsin Raza** for the valuable discussions that helped me to understand my research area in a much better way.

Acknowledgements are incomplete without paying regards to my parents and grandparents who've always given me perpetual love, care and cheers. Whose prayers have been a source of great inspiration for me and whose sustained hope in me led me to where I stand today. I have no words to thanks my beloved uncles **Prof. Dr. Muhammad Sajjad, Prof. Muhammad Masood** and **Mr. Muhammad Ishaq** who developed self-confidence and support me

**Muhammad Awais**



## Preface

The nanofluid is a fluid containing nanometer-sized (less than 100nm) particles, called nanoparticles. These fluids are engineered colloidal suspensions of nanoparticles in a base fluid. The nanoparticles used in nanofluids are typically made of metals, oxides, carbides, or carbon nanotubes. Nanofluids was first introduced by Choi [1] in 1995. Materials with nanometers sizes possess unique physical and chemical properties. It was found that the presence of nanoparticles within the fluid can appreciably increases the effective thermal conductivity of the fluid and as a result, increases the heat transfer characteristics [2].

MHD is a study of the interaction of electrically conducting fluids and electromagnetic forces. The MHD fluid was first introduced by Swedish Physicist, Alfven [3]. In recent years the study of MHD flow of an electrically conducting fluid past a heated surface has attracted the attention of many researchers. This is because of its considerable applications in many engineering problems such as plasma studies, petroleum industries, MHD power generators, cooling of nuclear reactors, the boundary layer control in aerodynamics and crystal growth. An applied magnetic field effect in natural convection flow of nanofluid is studied by Sheikholeslami et al. [4]. In this thesis simultaneous effects of MHD and porosity in Newtonian nanofluid on wavy surface are investigated. Mathematical modeling is based upon continuity, momentum and energy equations. The physical problems are first modeled and then the basic governing equations are reduced to a set of non-dimensional form by using appropriate transformations. The resulting equations are solved by using BVP4c 2.0 which is based on HAM in order to get exact solutions of nonlinear ODEs. The physical interpretations of sundry parameters such as nanoparticle concentration, porosity parameter, magnetic strength and skin-friction coefficient are illustrated by graphs. In addition, correlation of Nusselt number corresponding to active parameters are also presented.

A material having pores (voids) is described as porous medium filled with fluid (liquid or gas). Porosity measures the empty spaces in a porous medium and comes from the ratio of volume of voids over the total volume. Examples of porous media are beach sand, sandstone, limestone, rye bread, wood and human lung. However, foams are often also characterized using theme of porous media. Most of the time, a porous medium is described by its porosity and sometimes the other properties like

permeability, tensile strength and electrical conductivity are also measured as a respective aspects of its constituents (solid matrix and fluid) and the pores structure [5].

This thesis comprises three chapters. Detail description of each chapter is as follows: Chapter one includes some relevant definitions and governing equations of the subsequent chapters.

Chapter two includes the review work of the natural convection along a vertical wavy surface in a porous medium with variable properties and cross diffusion effects [6].

In chapter three, heat and mass flow of water in porous medium with spherical packing beds by improving physical properties by copper oxides particles under the effect of magnetic field over wavy surface is explored. The effects of porosity on physical properties along with nano-particles appearance are taken into account. To see flow behavior of heat in consequence of enhancement copper oxides concentration, stream and heat lines are strategized. The natures of velocity and temperature profiles of nanofluid are discussed graphically under influence of particle concentration, magnetic field strength and porosity. For physical interest, credible results in enhancement of convection heat transfer rate through nano-particles are presented in tabular form.

# Contents

<b>1</b>	<b>Basic of fluid dynamic</b>	<b>3</b>
1.1	Fluid.....	3
1.2	Types of fluids.....	3
1.2.1	Newtonian fluids.....	3
1.2.2	Nanofluids.....	3
1.3	Heat transfer.....	4
1.3.1	Modes of heat transfer.....	4
1.3.2	Conduction.....	4
1.3.3	Convection.....	5
1.3.4	Radiation.....	5
1.4	Porous medium.....	5
1.5	Megnetohydrodynamics.....	5
1.6	Darcy model.....	5
1.6.1	Forchheimer model.....	6
1.6.2	Ergun model.....	7
1.6.3	Brinkman model.....	7
1.7	Non-Darcy models.....	7
1.7.1	Non-Darcy (Forchheimer model).....	7
1.7.2	Steady non-Darcy MHD free convection along an impermeable vertical plate.....	8

<b>2</b>	<b>Natural convection along a vertical wavy surface in a porous medium with variable properties and cross diffusion effects</b>	<b>9</b>
2.1	Formulation of the problem.....	9
2.2	Solution of the problem.....	12
2.3	Results and discussion.....	14
2.4	Concluding remarks.....	25
<b>3</b>	<b>Simultaneous effects of MHD and porosity in Newtonian nanofluid on wavy surface</b>	<b>26</b>
3.1	Mathematical formulation of the problem.....	26
3.1.1	Flow model.....	26
3.2	Nano fluid modeling.....	28
3.3	Heat transfer coefficient.....	30
3.4	Solution of the problem.....	30
3.5	Results and discussion.....	32
3.6	Concluding remarks.....	39
	<b>References</b>	<b>40</b>

# Chapter 1

## Basic of fluid dynamic

This chapter comprises of some elementary definitions which may be useful for the better understanding of the next two chapters.

### 1.1 Fluid

Any substance which shows resistance to its internal molecular structure when external force applies. Liquids and gases are identified as fluid since they deform continuously in response to shear stress.

### 1.2 Types of fluids

#### 1.2.1 Newtonian fluid

Such fluid which obeys Newton's law of viscosity is called Newtonian fluid. Newton's law of viscosity is given by

$$\tau = \mu \frac{du}{dy} \quad (1.1)$$

Where,  $\tau$  is the shear stress,  $\mu$  is the viscosity of fluid,  $du/dy$  is the shear rate or velocity of gradient. Gases and most common liquids are tends to Newtonian fluids. Most common examples are Water, thin motor oil, air, sugar solutions, silicone, etc.

#### 1.2.2 Nanofluid

Nanofluid is a fluid containing nanometer-sized particles, called nanoparticles. These fluids are engineered colloidal suspensions of nanoparticles in a base fluid. The nanoparticles used in nanofluids are typically made of metals, oxides, carbides, or carbon nanotubes. Common base fluids include water and ethylene glycol.

## 1.3 Heat transfer

In physics, heat is the energy transferred from one body or system to another due to difference in temperature. The discipline of heat transfer is concerned with only two things one of them is temperature and the other is flow heat. Temperature represents the amount of thermal energy available, whereas, heat flow represent the movement of thermal energy from place to place.

### 1.3.1 Modes of heat transfer

Modes of heat transfer are mainly classified into three categories as given below.

### 1.3.2 Conduction

Conduction is a heat flow through solids without any visible movement of the particles. It is because of temperature difference in which heat transportations takes place from the more energetic particles to energetic fluid particles only by collision or because of molecular vibrations and the energy movement by free electrons. Heat transfer occurs in Silver, Copper, Mercury and Iron through conduction. Heat conduction rate depends upon the medium's geometry, relative thickness and the type of material. It can be easily measured in one dimension as flows

$$\left. \begin{aligned} \text{Heat conduction rate} &\propto \frac{(\text{area})(\text{temprature difference})}{\text{thickness}} \\ Q_{cond} &= k_f A \frac{T_1 - T_2}{\Delta x} \end{aligned} \right\} \quad (1.2)$$

The above equation is also called heat conduction equation in which proportionality constant  $k_f$  stand for material's thermal conductivity which measures the material's heat conducting capability. When  $\Delta x \rightarrow 0$  then the above equation becomes

$$Q_{cond} = -k_f A \frac{dt}{dx} \quad (1.3)$$

The above equality recognized as Fourier's law of heat conduction.

### **1.3.3 Convection**

Heat convection is the transportation and exchange of heat, due to mixing motion of different parts of fluid. It is governed by the laws of fluid dynamics in combination with the laws of heat conduction. Examples of convection are hot water, the cooling system of an automobile engine, the flow of the blood in human body etc.

### **1.3.4 Radiation**

Radiation is heat transfer mechanism in which heat transfer take place from any material through emission or absorption of electromagnetic waves. Especially radiation is significant during combustion processes where temperature is very high, but can also be favorable at room's temperature. The transfer of heat due to radiation can occur through gasses, fluids or a vacuum. Distinct from conductive and convective processes, heat transfer by radiative processes does not require to propagate any material.

## **1.4 Porous medium**

A material having pores (voids) is described as porous medium filled with fluid (liquid or gas). Porosity measures the empty spaces in a porous medium and comes from the ratio of volume of voids over the total volume. Examples of porous media are beach sand, sandstone, limestone, rye bread, wood and human lung. However, foams are often also characterized using theme of porous media. Most of the time, a porous medium is described by its porosity and sometimes the other properties like permeability, tensile strength and electrical conductivity are also measured as a respective aspects of its constituents (solid matrix and fluid) and the pores structure.

## **1.5 Magnetohydrodynamics (MHD)**

MHD is a discipline which studies the dynamics of electrically conducting fluids. The word magnetohydrodynamics (MHD) is derived from magneto-meaning magnetic field, hydro-meaning liquid, and dynamics meaning movements. The field of MHD was initiated by Hannes Alfvén for which he received the Noble prize in physics in 1970. Examples of such fluids include plasmas, liquid metal and salt water.

## **1.6 Darcy models**

The principle that governs how fluid moves in the subsurface is called Darcy's law. Darcy's law is an equation that defines the ability of a fluid to flow through a porous media such as

rock. It relies on the fact that the amount of flow between two points is directly related to the difference in pressure between the points, the distance between the points, and the interconnectivity of flow pathways in the rock between the points. The measurement of interconnectivity is called permeability. The law was formulated by Henry Darcy based on the results of experiments (published 1856) on the flow of water through beds of sand. It also forms the scientific basis of fluid permeability used in the earth sciences.

In 1856, H. Darcy investigated water flow through a sand column and found that the driving force and fluid transport obey the following relationship:

$$-\nabla p = \frac{\mu}{K} u, \quad (1.4)$$

where  $\nabla p$  is the pressure gradient,  $K$  the permeability and  $u$  the superficial velocity. In an external force field, Darcy's law may be extended as

$$-\nabla p + b = \frac{\mu}{K} u, \quad (1.5)$$

where  $b$  is a body force.

### 1.6.1 Forchheimer model

Darcy's law forms a basis for modeling fluid transport in porous media. In applications where fluid velocities are low, such as movements of groundwater and petroleum, etc., Darcy's law well describes the fluid transport in porous media. However, in applications where fluid velocities are high, the fluid transport predicted by Darcy's law usually departs from measurements considerably. Forchheimer (1901) might be the first to point out that the departure of predictions by Darcy's law from measurements may be due largely to the kinetic effect of fluid which is not included in the models for small Reynolds-number flows. For this reason, he suggested that a term representing the kinetic energy of fluid,  $\rho u^2$  be included in Eq. (1.5), i.e.,

$$-\nabla p = \frac{\mu}{K} u + a \rho u^2. \quad (1.6)$$

The added term is often referred to as the Forchheimer term in the literature. The parameter  $a$  is called the Forchheimer constant or parameter whereas  $\rho$  is the density. It may be



relevant to note that the Forchheimer term was also expressed in the form  $a\rho u^m$ , where  $m = 1.6-2.0$ .

## 1.6.2 Ergun model

The most widely used expression for  $a$  is that given by Ergun (1952),  $a = C_E / K^{1/2}$ , where  $C_E$  is the so-called Ergun constant. Although the Ergun constant is dimensionless, it is not a universal constant and is often found to vary with changes in porosity and structure of the porous medium. Ergun's version of Eq. (1.6) is

$$-\nabla p = \frac{\mu}{K} u + \frac{C_E}{K^{1/2}} \rho u^2. \quad (1.7)$$

The Ergun equation is often written in the vector form in the literature as,

$$-\nabla p = \frac{\mu}{K} u + \frac{C_E}{K^{1/2}} \rho |u| u. \quad (1.8)$$

## 1.6.3 Brinkman model

Another extension to the traditional form of Darcy's law is the Brinkman term (introduced by Brinkman in 1949), which is used to account for transitional flow between boundaries.

$$\beta_1 \nabla^2 q + q = \frac{-K}{\mu} \nabla p, \quad (1.9)$$

where  $\beta_1$  is an effective viscosity term. This correction term accounts for flow through medium where the grains of the media are porous themselves, but is difficult to use, and typically neglected.

## 1.7 Non-Darcy models

### 1.7.1 Non-Darcy (Forchheimer equation)

Forchheimer proposed a flow equation to account for the non-linear effect of turbulence by adding a second order term

$$\frac{-dp}{ds} = \frac{\mu_g}{K} \left( \frac{q_g}{A_1} \right) + \beta_2 \rho_g \left( \frac{q_g}{A_1} \right)^2. \quad (1.10)$$

Here  $\beta_2$  is Forchheimer coefficient,  $A_1$  is constant. As flow rate decreases, one approaches Darcy's Law (2nd order term approaches zero).

### 1.7.2 Steady non-Darcy MHD free convection along an impermeable vertical plate

$$\nabla p = \frac{\mu}{K}u + \rho Cu^2. \quad (1.11)$$

The permeability  $K$  and inertia coefficient  $C$  in this case are

$$K = \frac{d^2 \phi^3}{150(1-\phi)^2}, \quad (1.12)$$

$$C = \frac{1.75(1-\phi)}{d\phi^3}. \quad (1.13)$$

## Chapter 2

# Natural convection along a vertical wavy face in a porous medium with variable properties and cross diffusion effects

### Introduction

In this chapter, the effect of variable viscosity and variable thermal conductivity on free convective heat and mass transfer along a vertical wavy surface embedded in a Darcy porous medium in the presence of cross diffusion effects is review work of [6]. The wavy surface of the vertical plate is transformed into plane geometry case by using a suitable transformation and then solved numerically by employing the Runge-Kutta fourth order method with shooting technique. Numerical results for dimensionless flow velocity, temperature and concentration distribution as well as Nusselt number and Sherwood numbers are presented graphically for various values of Soret and Dufour parameters, variable viscosity, variable thermal conductivity parameters and amplitude of the wavy surface.

### 2.1 Formulation of the problem

The boundary layer flow near the wavy surface in a fluid saturated porous medium is considered. The wavy surface is described by

$$y^* = \sigma^*(x^*) = a^* \sin\left(\frac{\pi x^*}{l}\right), \quad (2.1)$$

here  $a^*$  is the amplitude of the wavy surface whereas  $l$  is the characteristics length of the wavy surface.

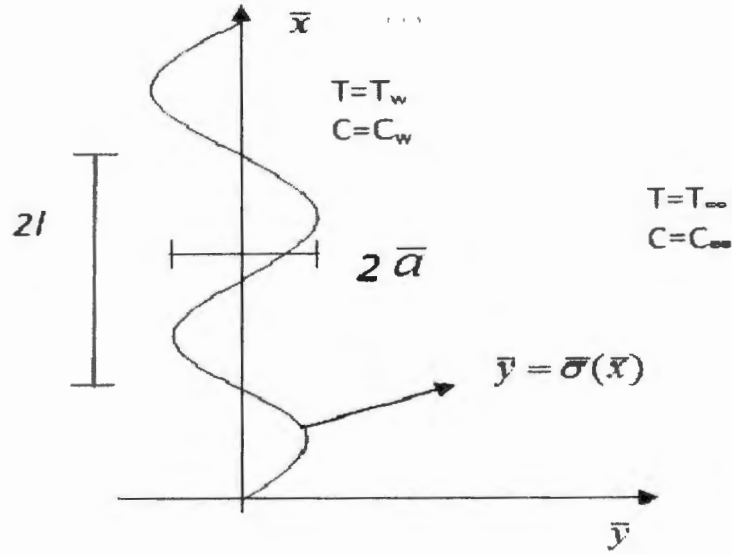


Fig 2.1: Physical model and coordinates

The governing equations under the Boussinesq approximation are given by [7]

$$\frac{\partial u^*}{\partial x^*} + \frac{\partial v^*}{\partial y^*} = 0, \quad (2.2)$$

$$\frac{\partial}{\partial y^*} \left( \frac{\mu}{K} u^* \right) = \frac{\partial}{\partial x^*} \left( \frac{\mu}{K} v^* \right) + \rho g \beta_t \frac{\partial T}{\partial y^*} + \rho g \beta_c \frac{\partial C}{\partial y^*}, \quad (2.3)$$

$$u^* \frac{\partial T}{\partial x^*} + v^* \frac{\partial T}{\partial y^*} = \frac{\partial}{\partial x^*} \left( \alpha \frac{\partial T}{\partial x^*} \right) + \frac{\partial}{\partial y^*} \left( \alpha \frac{\partial T}{\partial y^*} \right) + \frac{Dk_T}{c_s c_p} \left( \frac{\partial^2 C}{\partial (x^*)^2} + \frac{\partial^2 C}{\partial (y^*)^2} \right), \quad (2.4)$$

$$u^* \frac{\partial C}{\partial x^*} + v^* \frac{\partial C}{\partial y^*} = D \left( \frac{\partial^2 C}{\partial (x^*)^2} + \frac{\partial^2 C}{\partial (y^*)^2} \right) + \frac{Dk_T}{T_m} \left( \frac{\partial^2 T}{\partial (x^*)^2} + \frac{\partial^2 T}{\partial (y^*)^2} \right), \quad (2.5)$$

where  $u^*$  and  $v^*$  are the volume averaged velocity components in  $x^*$  and  $y^*$  directions, respectively.  $\beta_t$  is the coefficient of thermal expansion,  $\beta_c$  is the coefficient of concentration expansion,  $\alpha$  is the dimensional thermal conductivity,  $k_T$  is the thermal diffusion ratio,  $D$  is the mass diffusivity of the saturated porous medium,  $c_s$  is the concentration susceptibility,  $c_p$  is the specific heat at constant pressure,  $T_m$  is the mean fluid temperature and  $g$  is the gravitational acceleration. Fig. 2.1 shows that wavy surface is held at constant temperature  $T_w$  and constant concentration  $C_w$  which are higher than the porous medium temperature  $T_\infty$  and concentration  $C_\infty$  sufficiently far from the wavy surface.

The corresponding boundary conditions are

$$\begin{aligned} u^* = 0, \quad v^* = 0, \quad T = T_w, \quad C = C_w \quad \text{at} \quad y^* = \sigma^*(x^*) = a^* \sin\left(\frac{\pi x^*}{l}\right), \\ u^* \rightarrow 0, \quad T \rightarrow T_\infty, \quad C = C_\infty \quad \text{as} \quad y^* \rightarrow \infty. \end{aligned} \quad (2.6)$$

The fluid properties are assumed to be isotropic and constant, except for the fluid viscosity  $\mu$  and fluid thermal conductivity  $\alpha$ . The fluid viscosity  $\mu$  which is assumed to vary as an inverse linear function of the temperature  $T$  [8], as

$$\frac{1}{\mu} = \frac{1}{\mu_\infty} (1 + \delta(T - T_\infty)) \quad \text{or} \quad \frac{1}{\mu} = b(T - T_r), \quad (2.7)$$

here  $b = \frac{\delta}{\mu_\infty}$  and  $T_r = T_\infty - \frac{1}{\delta}$ . Both  $b$  and  $T_r$  are constants and their values depend on the reference state and the thermal property of the fluid i.e.,  $\delta$ . In general  $b > 0$  for liquids and  $b < 0$  for gases. The variable viscosity parameter  $\theta_r$ , which is defined by.

$$\theta_r = \frac{T_r - T_\infty}{T_w - T_\infty} = -\frac{1}{\delta(T_w - T_\infty)} \quad (2.8)$$

is constant. It is an important to note that for  $\delta \rightarrow 0$  (i.e.,  $\mu = \mu_\infty = \text{constant}$ ) then  $\theta_r \rightarrow \infty$ . It is also mentioning here that  $\theta_r$  is positive for gases and negative for liquids.  $T_\infty$  is the free stream temperature. Also, we assume that the fluid thermal conductivity  $\alpha$  is assumed to vary as a linear function of temperature in the form [9]:

$$\alpha = \alpha_o (1 + E (T - T_\infty)), \quad (2.9)$$

where  $\alpha_o$  is the thermal diffusivity at the wavy surface temperature  $T_w$  and  $E$  is a constant depending on the nature of the fluid. It is worth mentioning here that  $E < 0$  for fluids such as lubrication oils, while  $E > 0$  for fluids such as air, water. This can be written in the non-dimensional form [10] as

$$\alpha = \alpha_o (1 + \beta \theta), \quad (2.10)$$

in which  $\beta = E(T_w - T_\infty)$  is the thermal conductivity parameter and  $T_w$  is the wavy surface temperature. The variation of  $\beta$  can be taken in the range as  $-0.1 \leq \beta \leq 0$  for lubrication oils,  $0 \leq \beta \leq 0.12$  for water and  $0 \leq \beta \leq 6$  for air.

## 2.2 Solution of the problem

The stream function  $\psi^*$  is defined by

$$u^* = \frac{\partial \psi^*}{\partial y^*}, \quad v^* = -\frac{\partial \psi^*}{\partial x^*}. \quad (2.11)$$

Introducing the following non-dimensional variables

$$\left. \begin{aligned} (x, y, a, \sigma) &= (x^*, y^*, a^*, \sigma^*) / l, & \bar{\psi} &= \psi^* / \alpha_o, \\ \theta &= \frac{T - T_x}{T_w - T_x}, & \phi &= \frac{C - C_{\infty}}{C_w - C_{\infty}}, \end{aligned} \right\} \quad (2.12)$$

into Eqs. (2.3)-(2.5), we get

$$\frac{1}{\theta - \theta_r} \left( \frac{\partial \theta}{\partial y} \frac{\partial \bar{\psi}}{\partial y} + \frac{\partial \theta}{\partial x} \frac{\partial \bar{\psi}}{\partial x} \right) + \frac{\partial^2 \bar{\psi}}{\partial y^2} + \frac{\partial^2 \bar{\psi}}{\partial x^2} = Ra \left( 1 - \frac{\theta}{\theta_r} \right) \left( \frac{\partial \theta}{\partial y} + N \frac{\partial \phi}{\partial y} \right), \quad (2.13)$$

$$\frac{\partial \bar{\psi}}{\partial y} \frac{\partial \theta}{\partial x} - \frac{\partial \bar{\psi}}{\partial x} \frac{\partial \theta}{\partial y} = \beta \left( \left( \frac{\partial \theta}{\partial x} \right)^2 + \left( \frac{\partial \theta}{\partial y} \right)^2 \right) + (1 + \beta \theta) \left( \frac{\partial^2 \theta}{\partial x^2} + \frac{\partial^2 \theta}{\partial y^2} \right) + Du \left( \frac{\partial^2 \phi}{\partial x^2} + \frac{\partial^2 \phi}{\partial y^2} \right), \quad (2.14)$$

$$\frac{\partial \bar{\psi}}{\partial y} \frac{\partial \phi}{\partial x} - \frac{\partial \bar{\psi}}{\partial x} \frac{\partial \phi}{\partial y} = \frac{1}{Le} \left( \frac{\partial^2 \phi}{\partial x^2} + \frac{\partial^2 \phi}{\partial y^2} \right) + Sr \left( \frac{\partial^2 \theta}{\partial x^2} + \frac{\partial^2 \theta}{\partial y^2} \right). \quad (2.15)$$

Where  $Ra = \frac{g \beta_l K (T_w - T_x) l}{\alpha_o \nu}$  is the Darcy-Rayleigh number,  $\nu = \frac{\mu_o}{\rho}$  is the kinematic

viscosity of the fluid,  $N = \frac{\beta_c (C_w - C_{\infty})}{\beta_l (T_w - T_x)}$  is the buoyancy ratio,  $Le = \frac{\alpha_o}{D}$  is the Lewis

number,  $Du = \frac{Dk_T \Delta C}{\alpha_o c_s c_p \Delta T}$  is Dufour parameter and  $Sr = \frac{Dk_T \Delta T}{\alpha_o T_m \Delta C}$  is the Soret parameter.

The corresponding boundary conditions are given by

$$\left. \begin{aligned} \bar{\psi} &= 0, & \theta &= 1, & \phi &= 1 & \text{on } y &= a \sin x. \\ \bar{\psi}_y &\rightarrow 0, & \theta &\rightarrow 0, & \phi &\rightarrow 0 & \text{as } y &\rightarrow \infty. \end{aligned} \right\} \quad (2.16)$$

The effects of the wavy surface from the boundary conditions into the governing equations can be transferred by the following group of coordinate transformation

$$x = \xi, \quad y = \xi^{1/2} Ra^{-1/2} \eta + a \sin x, \quad \bar{\psi} = Ra^{1/2} \psi. \quad (2.17)$$

For boundary layer approximations, substitute Eq. (2.17) into Eqs. (2.13)-(2.15) and letting  $Ra \rightarrow \infty$ , we get

$$\frac{1}{\theta - \theta_r} (1 + a^2 \cos^2 \xi) \frac{\partial \theta}{\partial \eta} \frac{\partial \psi}{\partial \eta} + (1 + a^2 \cos^2 \xi) \frac{\partial^2 \psi}{\partial \eta^2} = \xi^{1/2} \left( 1 - \frac{\theta}{\theta_r} \right) \left( \frac{\partial \theta}{\partial \eta} + N \frac{\partial \psi}{\partial \eta} \right), \quad (2.18)$$

$$\begin{aligned} \xi^{1/2} \left( \frac{\partial \psi}{\partial \eta} \frac{\partial \theta}{\partial \xi} - \frac{\partial \psi}{\partial \xi} \frac{\partial \theta}{\partial \eta} \right) &= \beta (1 + a^2 \cos^2 \xi) \left( \frac{\partial \theta}{\partial \eta} \right)^2 + (1 + \beta \theta) (1 + a^2 \cos^2 \xi) \frac{\partial^2 \theta}{\partial \eta^2} \\ &+ Du (1 + a^2 \cos^2 \xi) \frac{\partial^2 \phi}{\partial \eta^2}, \end{aligned} \quad (2.19)$$

$$\xi^{1/2} \left( \frac{\partial \psi}{\partial \eta} \frac{\partial \phi}{\partial \xi} - \frac{\partial \psi}{\partial \xi} \frac{\partial \phi}{\partial \eta} \right) = \frac{1}{Le} (1 + a^2 \cos^2 \xi) \frac{\partial^2 \phi}{\partial \eta^2} + Sr (1 + a^2 \cos^2 \xi) \frac{\partial^2 \theta}{\partial \eta^2}. \quad (2.20)$$

For the system of ordinary differential equations, let us introduce the following similarity transformations

$$\hat{\eta} = \frac{\eta}{1 + a^2 \cos^2 \xi}, \quad \psi = \xi^{1/2} f(\hat{\eta}), \quad \theta = \theta(\hat{\eta}) \quad \text{and} \quad \phi = \phi(\hat{\eta}). \quad (2.21)$$

After using above transformations into Eqs. (2.18)-(2.20), we obtain

$$f'' + \frac{1}{\theta - \theta_r} \theta' f' = \left( 1 - \frac{\theta}{\theta_r} \right) (\theta' + N \phi'), \quad (2.22)$$

$$\beta (\theta')^2 + (1 + \beta \theta) \theta'' + \frac{1}{2} f \theta' + Du \phi'' = 0, \quad (2.23)$$

$$\frac{1}{Le} \phi'' + \frac{1}{2} f \phi' + Sr \theta'' = 0. \quad (2.24)$$

Subject to the boundary conditions

$$\left. \begin{aligned} f = 0, \quad \theta = 1, \quad \phi = 1 \quad \text{at} \quad \hat{\eta} = 0, \\ f' \rightarrow 0, \quad \theta \rightarrow 0, \quad \phi \rightarrow 0 \quad \text{as} \quad \hat{\eta} \rightarrow \infty \end{aligned} \right\} \quad (2.25)$$

Where prime denotes differentiation with respect to  $\hat{\eta}$ .

The rate of heat transfer (local Nusselt number) and rate of mass transfers (local Sherwood number) are defined as

$$Nu_x = \frac{-\theta'(0) Ra x^{1/2}}{(1 + a^2 \cos^2 x)^{1/2}}, \quad Sh_x = \frac{-\phi'(0) Ra x^{1/2}}{(1 + a^2 \cos^2 x)^{1/2}}. \quad (2.26)$$

### 2.3 Results and discussion

The set of nonlinear non-homogeneous differential Eqs. (2.22)-(2.24) with corresponding boundary conditions (2.25) are solved numerically using a shooting technique along with fourth order Runge-Kutta integration. In order to assess the accuracy of the present numerical method, obtained results are compared with those of Cheng [1] in the absence of fluid viscosity parameter, thermal conductivity parameter, Soret and Dufour parameter. The effect of various parameters on velocity, temperature and concentration fields have been presented in Figs. (2.2)-(2.20) and analyzed. The effect of variable viscosity  $\theta_r$  on the velocity, temperature and concentration profiles with respect to  $\eta$  is shown in Figs. (2.2)-(2.4). With increasing variable viscosity parameter ( $\theta_r$ ), the fluid boundary layer, thermal and solutal boundary layer thickness gradually reduced, which in turns causes to decrease velocity, temperature and concentration profiles. This can be explained physically as the parameter ( $\theta_r$ ) increases, the fluid viscosity increases resulting the depreciation in the boundary layer thickness.

The effect of thermal conductivity parameter  $\beta$  on the velocity, temperature and concentration profiles with respect to  $\eta$  are given in Figs. (2.5)-(2.7). Fig. (2.5) shows that increasing thermal conductivity parameter retards the flow considerably and hence it reduces the velocity boundary layer. From Fig. (2.6), it is clear that increasing values of  $\beta$  tends to increase the temperature profile due to increase in thermal boundary layer thickness. Fig. (2.7) reveals that with increasing  $\beta$ , concentration profile is found to decrease, that is  $\beta$  causes to reduce solutal boundary layer thickness.

The effect of Dufour parameter ( $Du$ ) on the velocity, temperature and concentration profiles with respect to  $\eta$  is shown in Figs. (2.8)-(2.10). From Fig. (2.8), it is note worthy that increasing Dufour parameter is to increase the velocity profile throughout the boundary layer. In Fig. (2.9), it is seen that the temperature profile increases with increasing values of Dufour parameter, leading to an increase in thermal boundary layer thickness. In Fig. (2.10), an increase in Dufour parameter causes a slight decrease in solutal boundary layer thickness, which turns to reduce the concentration profile. It is an important to note that temperature is highest at leading edge of the plate and asymptotically decrease to zero far away from the plate with boundary condition.

The effect of Soret parameter ( $Sr$ ) on the velocity, temperature and concentration profiles with respect to  $\eta$  is shown in Figs. (2.11)-(2.13). From these figs we observe that as increase



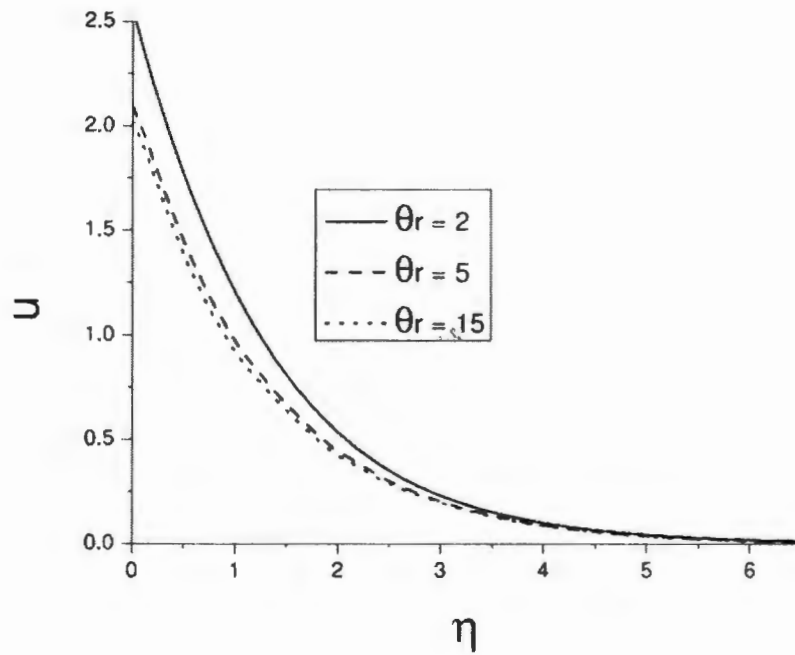
in Soret parameter due to the contribution of the temperature gradients to species diffusion, results an enhancement in velocity, temperature and concentration profiles. It is noticed from these figs that velocity, temperature and concentration of fluid particle value of 1 at the plate surface and then decrease slowly till it attains the minimum value of zero far away from the plate surface with increasing value of Soret parameter.

Fig. (2.14) illustrates the stream wise profile of the local Nusselt number for various values of  $\theta_r$ . This shows that increasing the  $\theta_r$  reduces the fluctuation of local Nusselt number with the stream wise coordinate  $\zeta$ . Fig.(2.15) shows the effect of  $\theta_r$  on local Sherwood number. It is clear that increasing the  $\theta_r$  leads to a smaller fluctuations of the local Sherwood number with stream wise coordinate  $\zeta$ . For a value of  $\zeta$ , Nusselt number and Sherwood number decreases with increase in  $\theta_r$ .

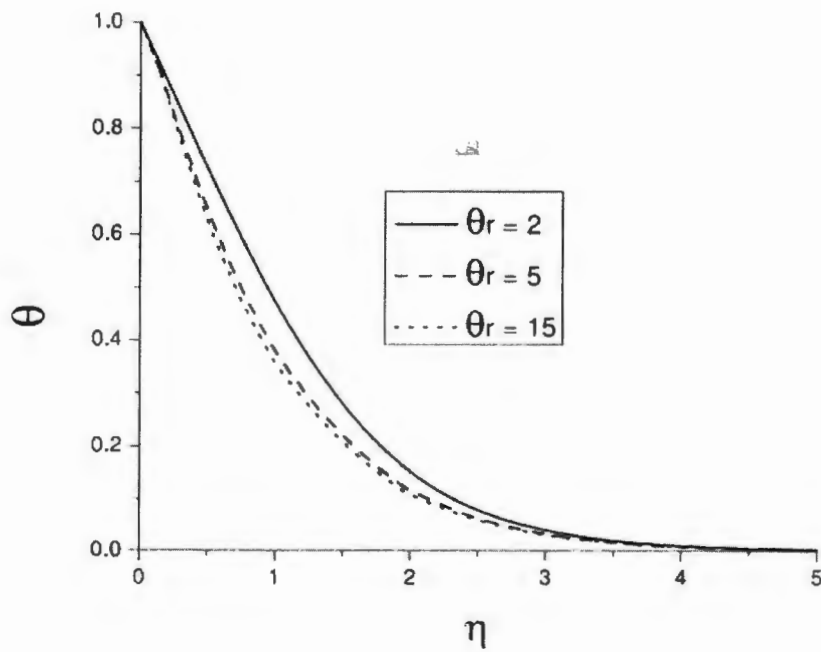
Fig.(2.16) plots the stream wise distribution of the local Nusselt number for different values of variable thermal conductivity. Results show that increase in the variable thermal conductivity leads to smaller fluctuations of the local Nusselt number with the stream wise coordinate  $\zeta$ . Fig. (2.17) shows the stream wise distribution of the local Sherwood number for various values of variable thermal conductivity parameter. It is observed that greater fluctuations of the local Sherwood number with increasing values of variable thermal conductivity parameter with stream wise coordinate  $\zeta$ . In addition, for a value of  $\zeta$ , Nusselt number decreases and Sherwood number increases with increasing values of  $\beta$ .

Fig. (2.18) shows the stream wise distribution of the local rate of heat transfer for different values of Dufour parameter. As the Dufour parameter increases the fluctuations of the local rate of heat transfer with stream wise coordinate  $\zeta$  is reduced. In addition, we observed that increase in Dufour parameter tends to increase the rate of heat transfer as increase in  $\zeta$ . Fig. (2.19) depicts the stream wise distribution of the local sherwood number for various values of Dufour effect. It is observed that increase in the Dufour effect leads to a greater fluctuations of the local Sherwood number. Moreover, the Sherwood number increases with increasing values of Dufour parameter as  $\zeta$  value increase.

The effect Soret parameter on Nusselt number is exhibits in Fig. (2.20). From this fig it is observed that increasing the Soret parameter results greater fluctuation in local Nusselt number with stream wise coordinate  $\zeta$ . i.e., the rate of heat transfer increases with increasing values of Soret parameter.



**Fig 2.2:** Velocity profile for different values of  $\theta_r$  for  $\beta = 0.5$ ,  $N = 1$ ,  $Le = 1$ ,  $Sr = 1$  and  $Du = 0.1$ .



**Fig 2.3:** Temperature profile for different values of  $\theta_r$  for  $\beta = 0.5$ ,  $N = 1$ ,  $Le = 1$ ,  $Sr = 1$  and  $Du = 0.1$ .

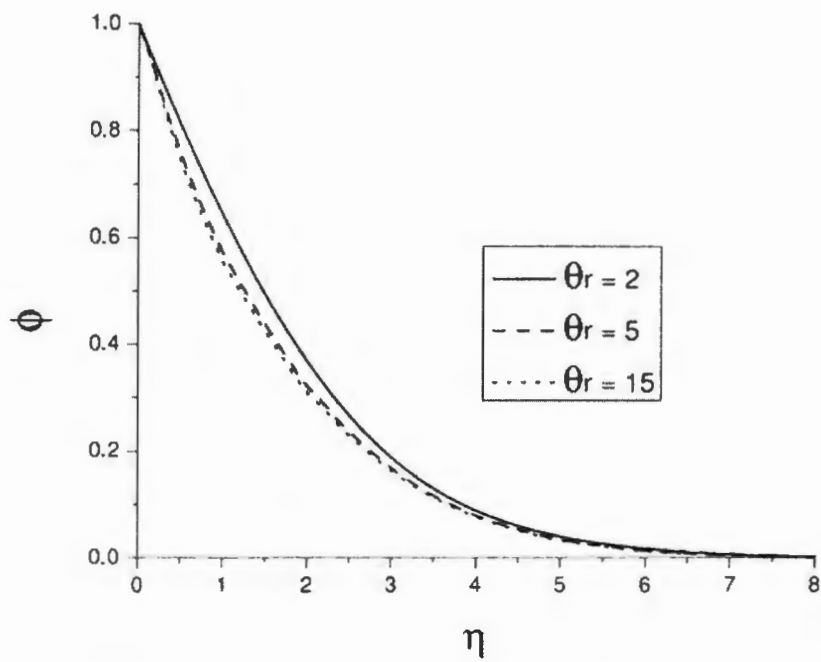


**Fig 2.4:** Concentration profile for different values of  $\theta_r$  for  $\beta = 0.5$ ,  $N = 1$ ,  $Le = 1$ ,  $Sr = 1$  and  $Du = 0.1$ .

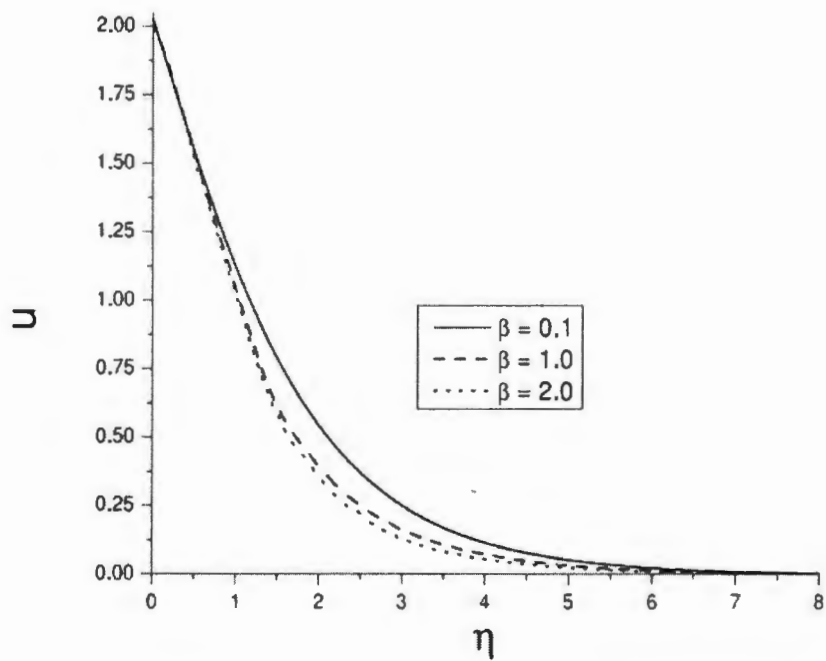


**Fig 2.5:** Velocity profile for different values of  $\beta$  for  $\theta_r = 15$ ,  $N = 1$ ,  $Le = 1$ ,  $Sr = 1$  and  $Du = 0.1$ .

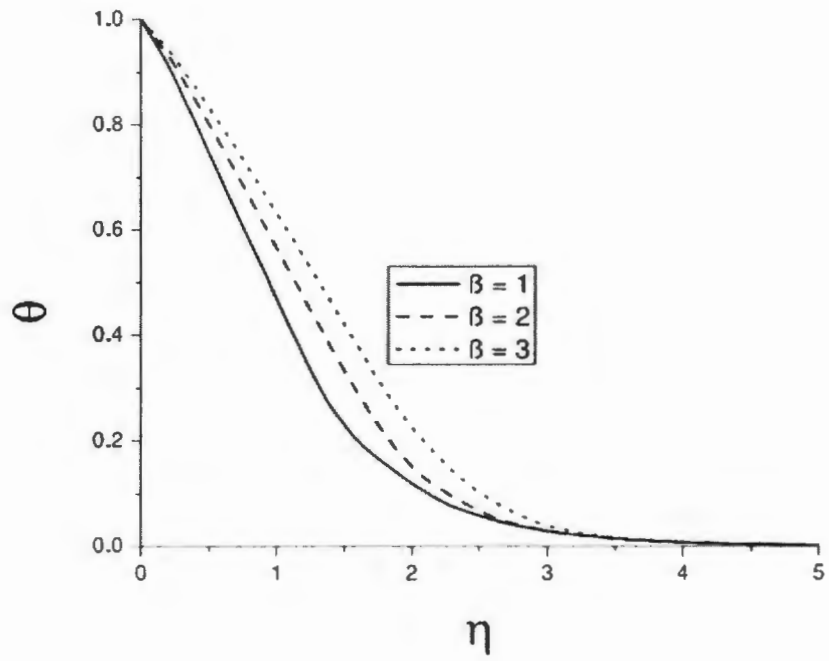


**Fig 2.6:** Temperature profile for different values of  $\beta$  for  $\theta_r = 15$ ,  $N = 1$ ,  $Le = 1$ ,  $Sr = 1$  and  $Du = 0.1$ .

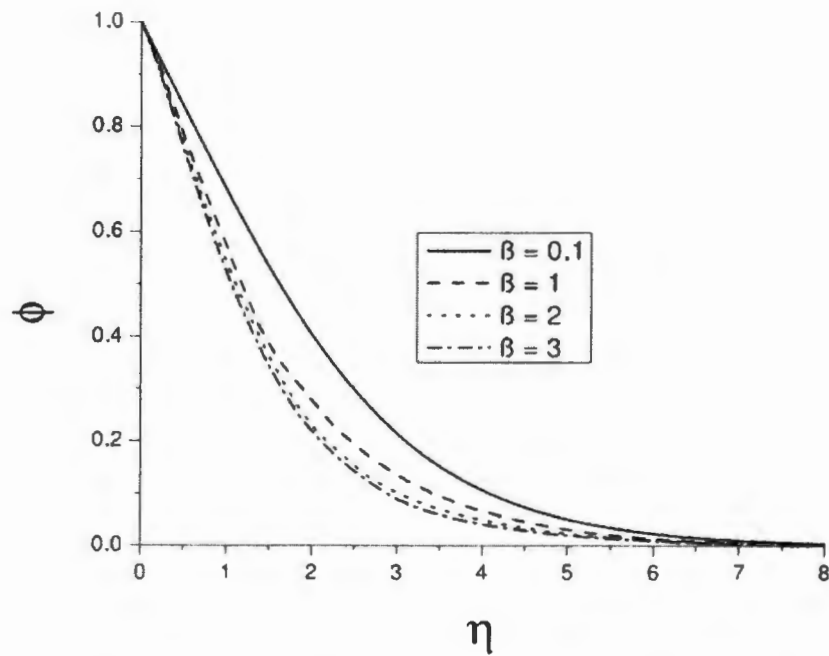


**Fig 2.7:** Concentration profile for different values of  $\beta$  for  $\theta_r = 15$ ,  $N = 1$ ,  $Le = 1$ ,  $Sr = 1$  and  $Du = 0.1$ .

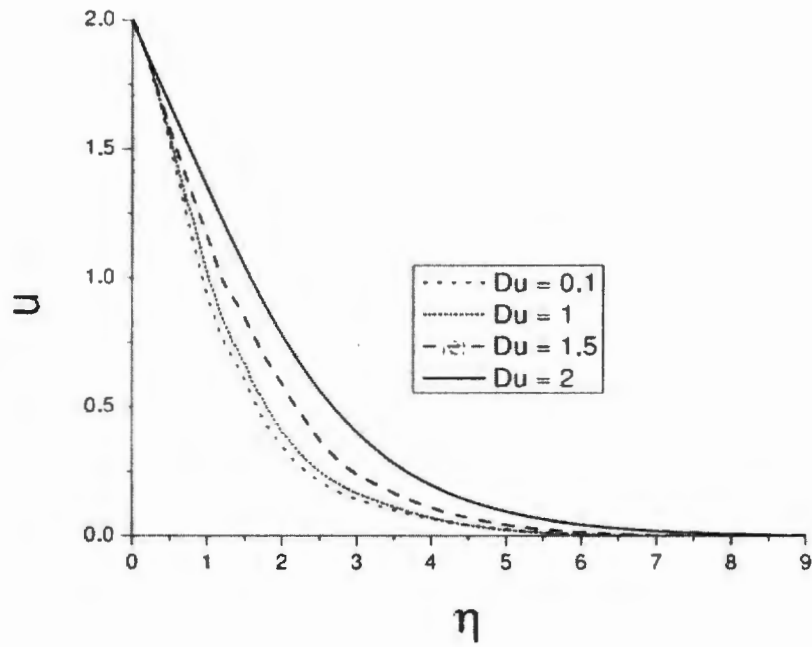


**Fig 2.8:** Velocity profile for different values of  $Du$  for  $\theta_r = 15$ ,  $N = 1$ ,  $Le = 1$ ,  $Sr = 1$  and  $\beta = 0.5$ .

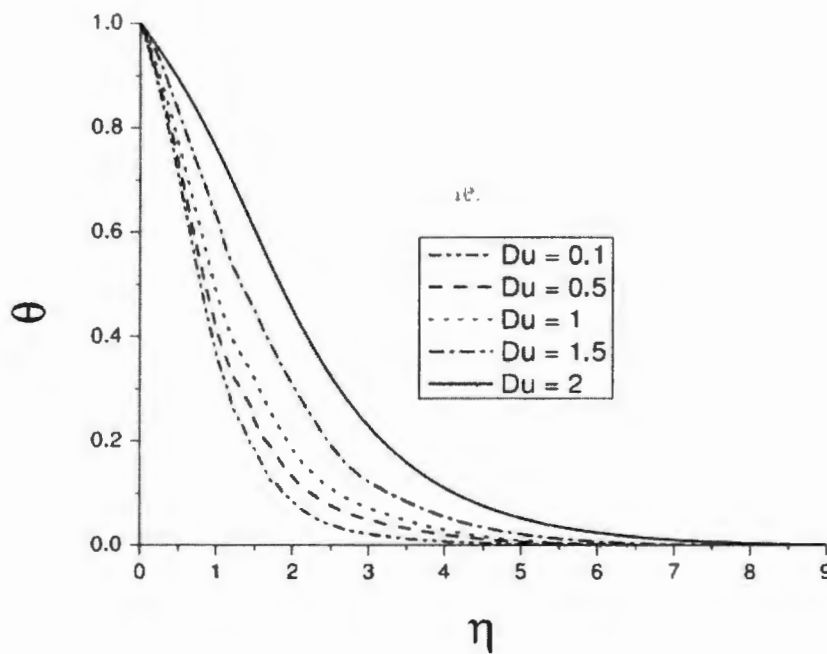


**Fig 2.9:** Temperature profile for different values of  $Du$  for  $\theta_r = 15$ ,  $N = 1$ ,  $Le = 1$ ,  $Sr = 1$  and  $\beta = 0.5$ .

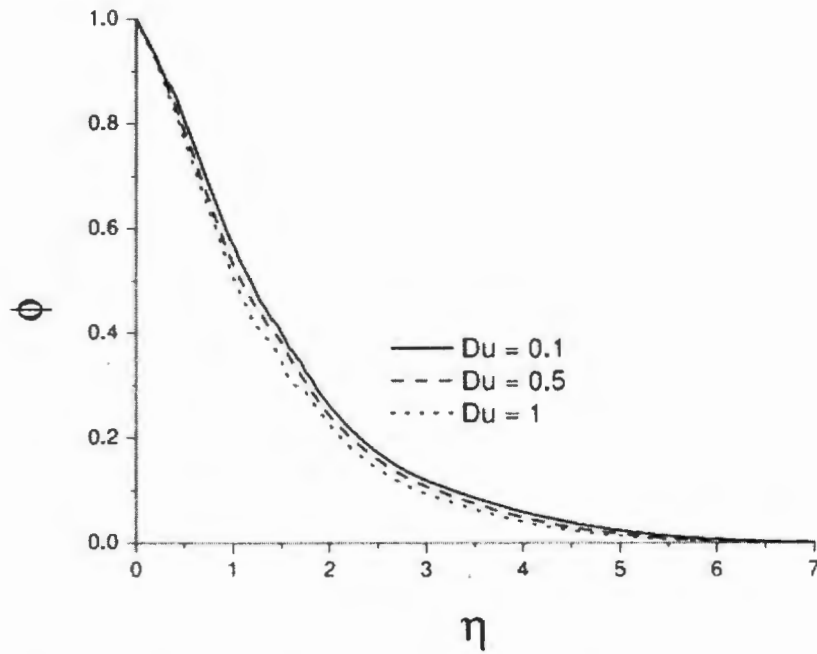


**Fig 2.10:** Concentration profile for different values of  $Du$  for  $\theta_r = 15$ ,  $N = 1$ ,  $Le = 1$ ,  $Sr = 1$  and  $\beta = 0.5$ .

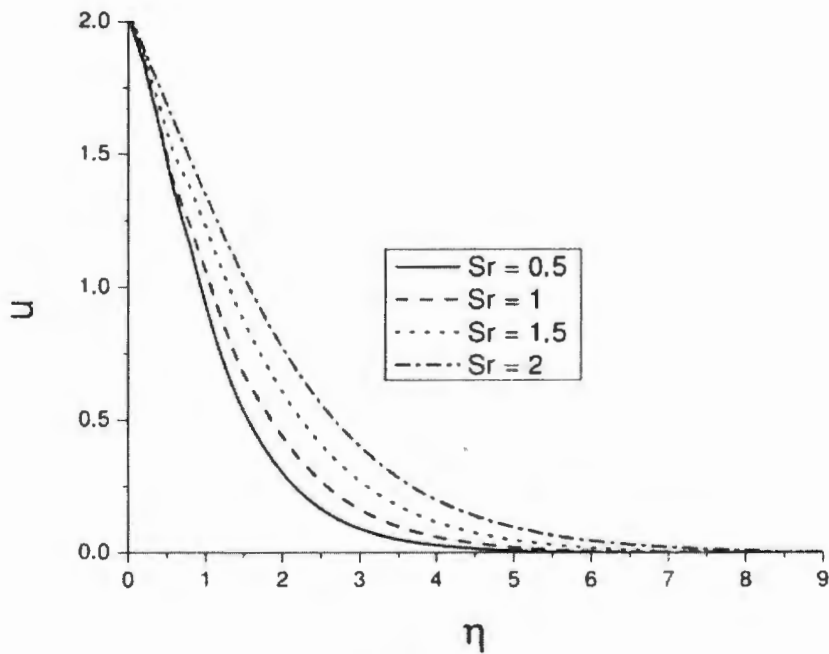


**Fig 2.11:** Velocity profile for different values of  $Sr$  for  $\theta_r = 15$ ,  $N = 1$ ,  $Le = 1$ ,  $Du = 0.1$  and  $\beta = 0.5$ .

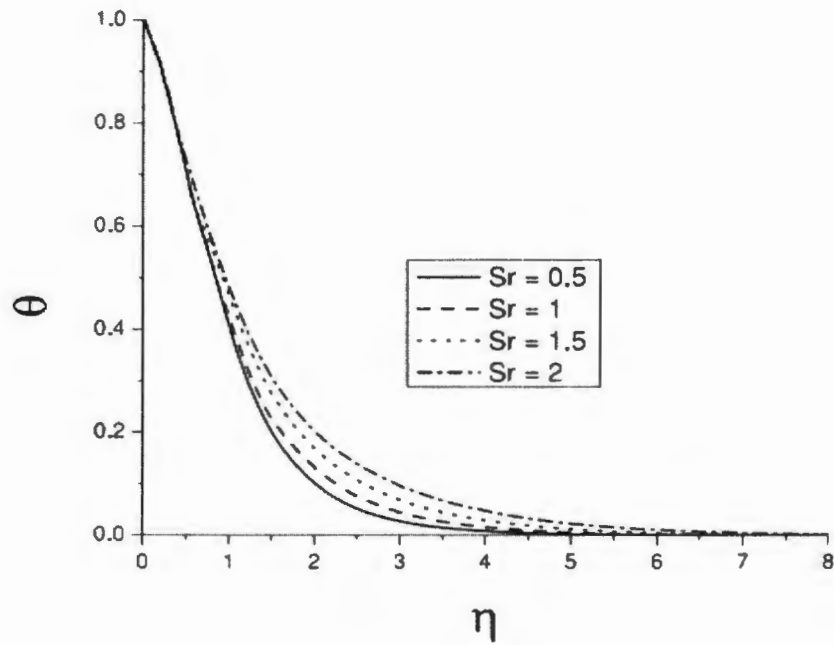


**Fig 2.12:** Temperature profile for different values of  $Sr$  for  $\theta_r = 15$ ,  $N = 1$ ,  $Le = 1$ ,  $Du = 0.1$  and  $\beta = 0.5$ .

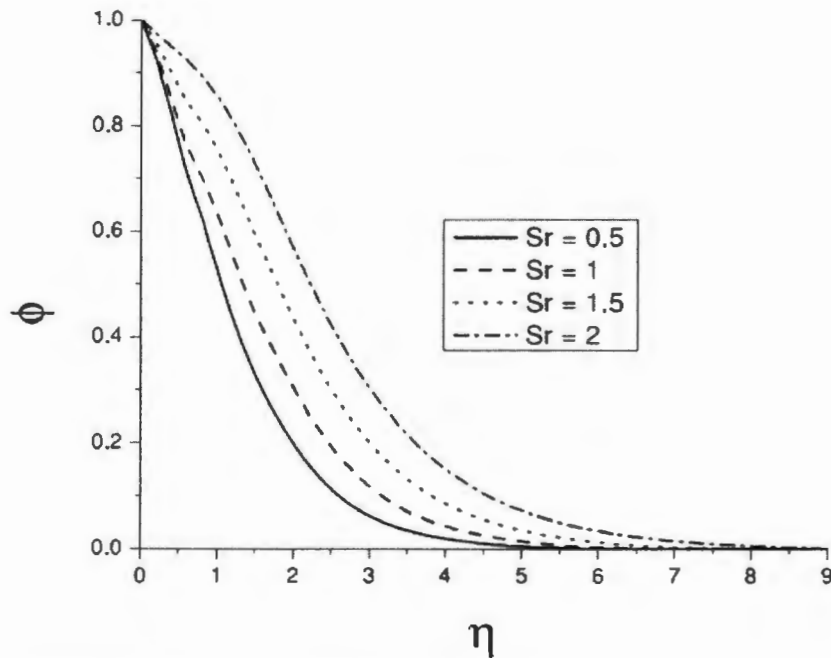


**Fig 2.13:** Concentration profile for different values of  $Sr$  for  $\theta_r = 15$ ,  $N = 1$ ,  $Le = 1$ ,  $Du = 0.1$  and  $\beta = 0.5$ .

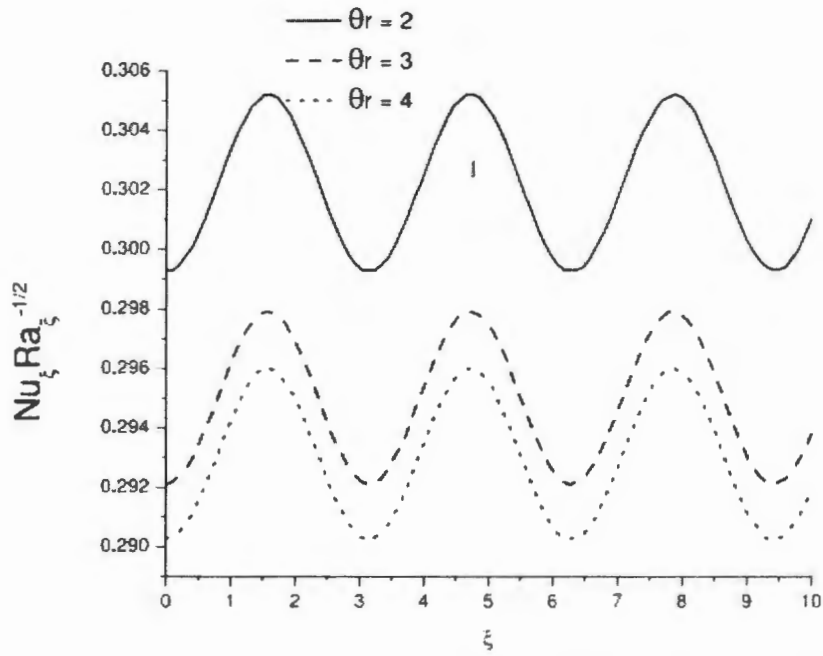


**Fig 2.14:** Local Nusselt number verses  $\xi$  for various values of  $\theta_r$  for  $Sr = 1$ ,  $N = 1$ ,  $Le=1$ ,  $Du = 0.1$ ,  $a = 0.5$  and  $\beta = 0.5$ .

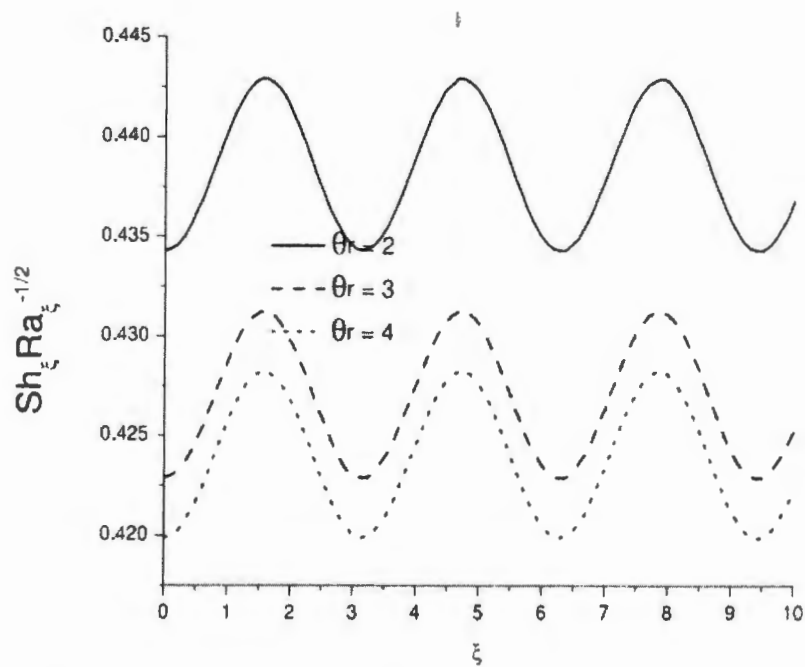


**Fig 2.15:** Local Sherwood number verses  $\xi$  for various values of  $\theta_r$  for  $Sr = 1$ ,  $N = 1$ ,  $Le=1$ ,  $Du = 0.1$ ,  $a = 0.5$  and  $\beta = 0.5$ .



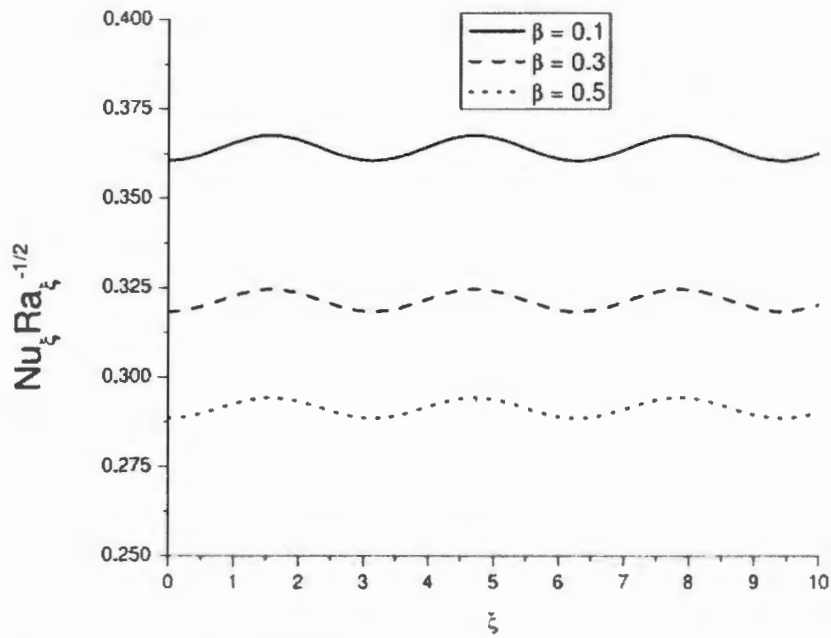


**Fig 2.16:** Local Nusselt number verses  $\xi$  for various values of  $\beta$  for  $Sr = 1$ ,  $N = 1$ ,  $Le = 1$ ,  $Du = 0.1$ ,  $a = 0.5$  and  $\theta = 3$ .

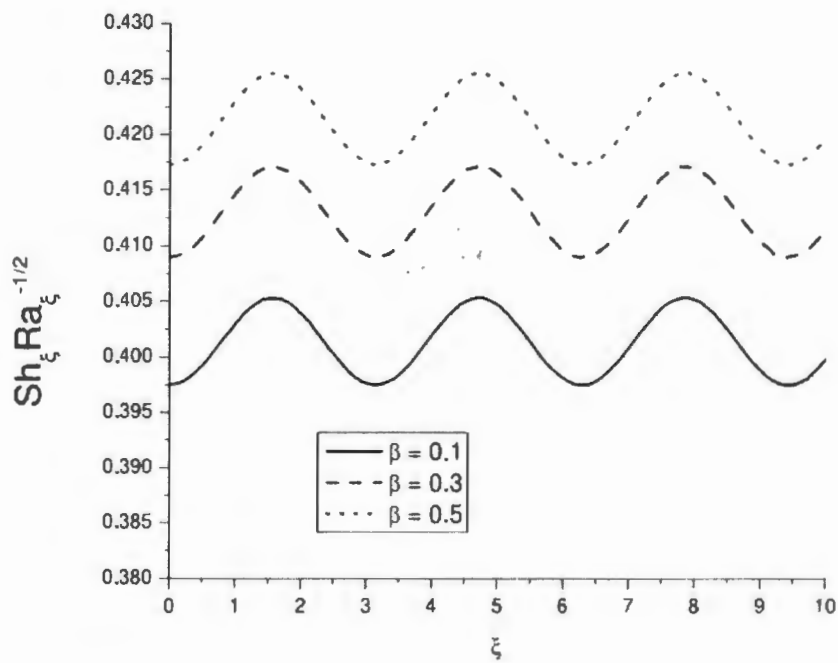


**Fig 2.17:** Local Sherwood number verses  $\xi$  for various values of  $\beta$  for  $Sr = 1$ ,  $N = 1$ ,  $Le = 1$ ,  $Du = 0.1$ ,  $a = 0.5$  and  $\theta = 3$ .

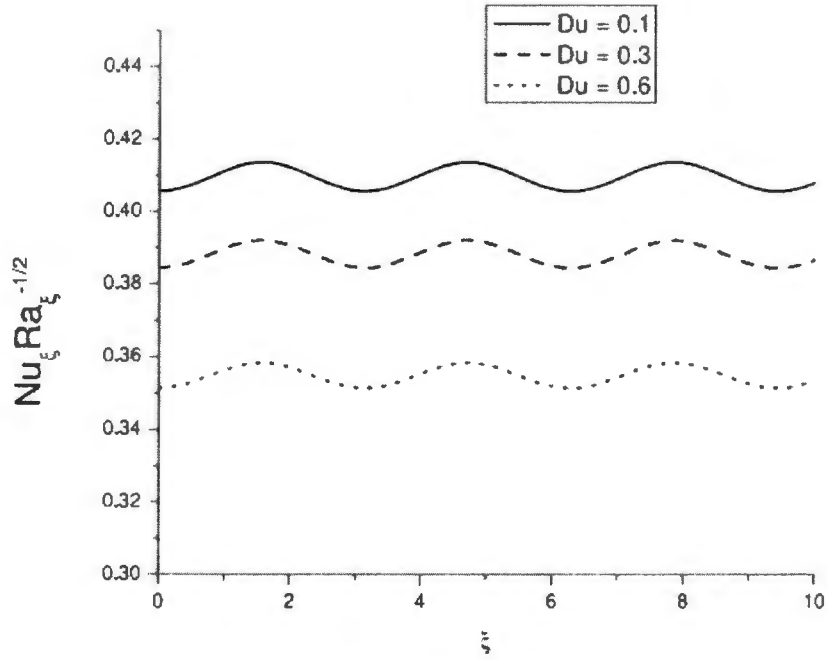


**Fig 2.18:** Local Nusselt number verses  $\xi$  for various values of  $Du$  for  $Sr = 1$ ,  $N = 1$ ,  $Le = 1$ ,  $\beta = 0.5$ ,  $a = 0.5$  and  $\theta = 3$ .

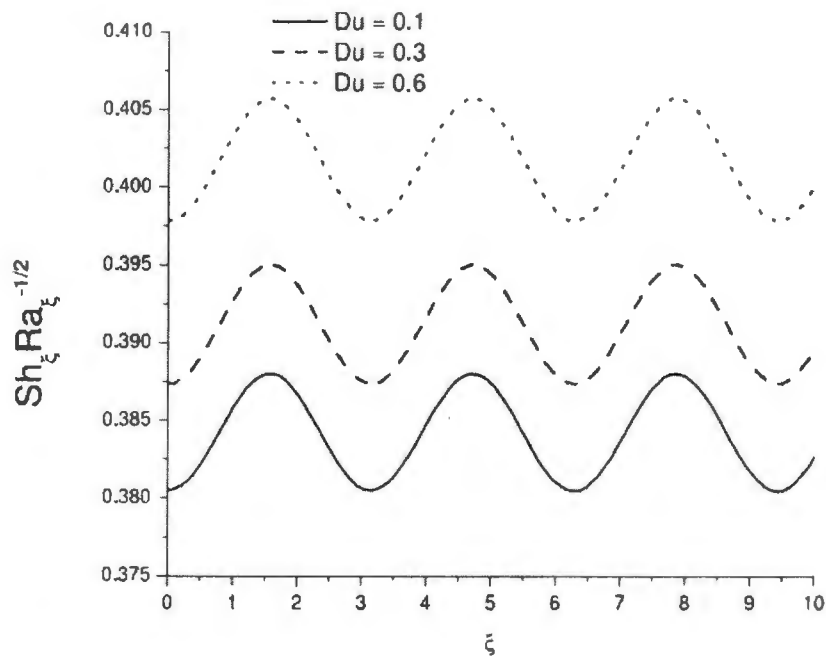


**Fig 2.19:** Local Sherwood number verses  $\xi$  for various values of  $Du$  for  $Sr = 1$ ,  $N = 1$ ,  $Le = 1$ ,  $\beta = 0.5$ ,  $a = 0.5$  and  $\theta = 3$ .

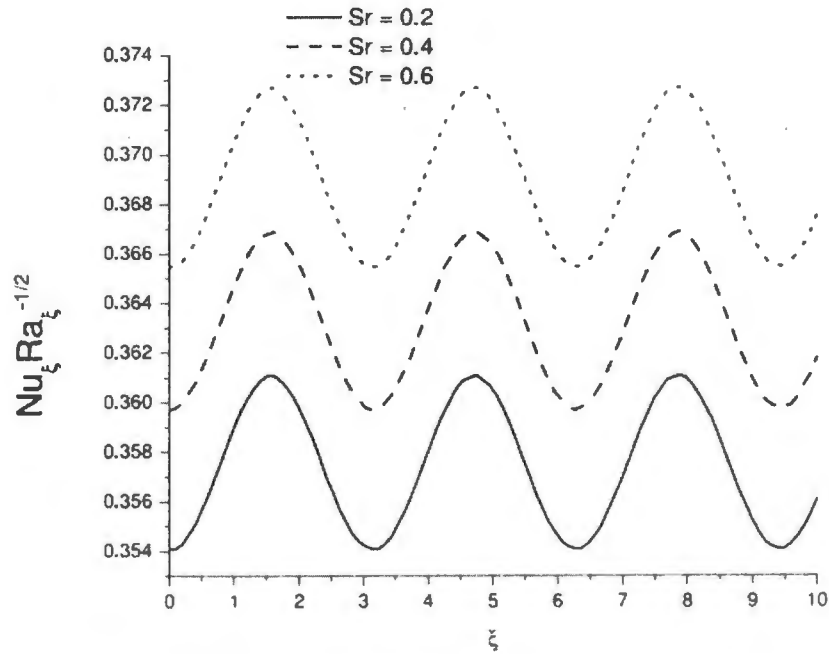


**Fig 2.20:** Local Nusselt number verses  $\zeta$  for various values of  $Sr$  for  $Du = 0.1$ ,  $N = 1$ ,  $Le = 1$ ,  $\beta = 0.5$ ,  $a = 0.5$  and  $\theta = 3$ .

## 2.4 Concluding remarks

The influence of variable properties and cross diffusion on steady convective heat and mass transfer flow over a vertical wavy surface embedded in a fluid saturated porous medium is investigated. The Fourth order Runge-Kutta method with Shooting technique is employed to solve the boundary layer equations and the numerical results are presented to analyze to fluid flow velocity, heat and mass transfer characteristics, Nusselt number and Sherwood number for various physical parameters. The main findings of the reviewed study are as follows:

1. An increase in variable viscosity  $\theta_r$ , decelerate the flow velocity, temperature, concentration and Nusselt number but enhance the Sherwood number.
2. An increase in thermal conductivity parameter  $\beta$  enhance the temperature and Sherwood number but decrease in velocity, concentration and Nusselt number.
3. As increase in Dufour parameter resulting in higher velocity, temperature and Sherwood number but decrease in concentration and Nusselt number. Velocity, temperature and concentration increase due to increase in Soret parameter.

## Chapter 3

### Simultaneous effects of MHD and porosity in

### Newtonian nanofluid on wavy surface

In this chapter, the heat distribution along mass flow of water in porous medium with spherical packing beds by improving physical properties by copper oxides particles under the effect of magnetic field over wavy surface is investigated. The effects of porosity and MHD on physical properties are taken along with nano-particles appearance. To see flow behavior of mass and heat in consequence of enhancement copper oxides concentration, stream and heat lines are strategized. The natures of velocity and temperature profiles of nanofluid are discussed graphically under influence of particle concentration, magnetic field strength and porosity. For physical interest, credible results in enhancement of convection heat transfer rate through nano-particles are calculated in tabular form.

### 3.1 Mathematical formulation

#### 3.1.1 Flow modeling

Consider the non-Darcy flow of nanofluid under magnetic effect along vertical wavy surface embedded in a thermally stratified. The surface temperature is varied according to the power-law form as  $T_w(x) = T_{\infty,0} + A_2 x^n$  and greater than ambient fluid temperature. The dimensional coordinate along the plate is denoted by  $x$  and that normal to it is denoted by  $y$  as shown in Fig. 3.1.

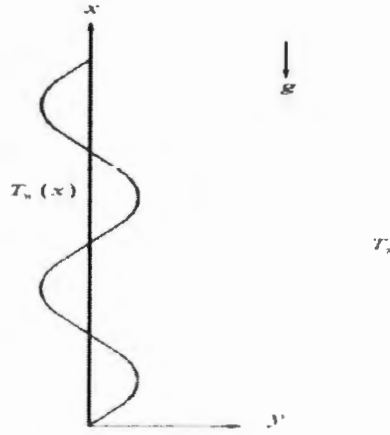


Fig. 3.1: Geometry of the problem.

The fluid and the porous structure are everywhere in local thermodynamic equilibrium. No chemical reactions are taking place in the flow. Under these assumptions taking into account Boussinesq and boundary layer approximations, the governing equations are obtained [11] as

$$\frac{\partial u}{\partial x} + \frac{\partial v}{\partial y} = 0, \quad (3.1)$$

$$\frac{\mu_{nf}}{K} u + \rho_{nf} C_1 u^2 = \frac{\mu_{nf}}{\varepsilon} \frac{\partial^2 u}{\partial y^2} + g(\rho\beta)_{nf} (T - T_\infty) - \sigma_{nf} \beta_o^2 u, \quad (3.2)$$

$$(\rho C_p)_{nf,eff} \left( u \frac{\partial T}{\partial x} + v \frac{\partial T}{\partial y} \right) = k_{nf,eff} \frac{\partial^2 T}{\partial y^2}. \quad (3.3)$$

The boundary conditions can be written as

$$\left. \begin{aligned} u = v = 0, \quad T = T_w(x) = T_{\infty,0} + A_2 x^n \quad \text{at} \quad y = \sigma(x) = \text{Sin}x \\ u = 0, \quad T = T_\infty \quad \text{as} \quad y \rightarrow \infty \end{aligned} \right\}, \quad (3.4)$$

where  $A_2$  is constant,  $T_\infty$  is the ambient temperature. For  $T_w > T_\infty$  the wall temperature increases in flow direction for positive  $n$  and decreases for negative  $n$ .

The permeability  $K$  and the Forchheimer coefficient  $C_1$  are determined from [11] as

$$K = \frac{d^2 \varepsilon^3}{150(1-\varepsilon)^2}, \quad (3.5)$$

$$C_1 = \frac{1.75(1-\varepsilon)}{d\varepsilon^3}, \quad (3.6)$$

here  $d$  is the particle diameter. The parameter  $\varepsilon$  shows the porosity of a packed-sphere bed.

Now, using the following similarity transformation

$$\begin{aligned} \eta &= \frac{y-\sigma(x)}{x} Gr_x^{1/4}, \quad \psi(x,y) = v_f Gr_x^{1/4} f(\eta), \\ u &= \frac{\partial \psi}{\partial y}, \quad v = -\frac{\partial \psi}{\partial x}, \quad \theta(\eta) = \frac{T-T_\infty}{T_w-T_\infty}, \end{aligned} \quad (3.7)$$

into Eqs. (3.2) and (3.3) and boundary conditions (3.4), dimensionless nonlinear system of ordinary differential equations takes the following forms

$$\frac{\mu_{nf}}{\mu_f} \frac{1}{\Lambda} f'' + \frac{\rho_{nf}}{\rho_f} C f'^2 = \frac{1}{\varepsilon} \frac{\mu_{nf}}{\mu_f} f''' + \frac{(\rho\beta)_{nf}}{(\rho\beta)_f} \theta - \frac{\sigma_{nf}}{\sigma_f} M f', \quad (3.8)$$

$$\frac{k_{nf,\sigma}}{k_f} \theta'' + \frac{(\rho C_p)_{nf,\sigma}}{(\rho C_p)_f} Pr f \theta' = 0. \quad (3.9)$$

$$\left. \begin{aligned} f &= 0, \quad f' = 0, \quad \theta = 1 \quad \text{at} \quad \eta \rightarrow 0 \\ f' &= 0, \quad \theta = 0 \quad \text{at} \quad \eta \rightarrow \infty \end{aligned} \right\} \quad (3.10)$$

In above  $\Lambda = \frac{K Gr_x^{1/2}}{x^2}$  is dimensionless permeability parameter and  $C = C_1 x$  is dimensionless Forchheimer coefficient.

### 3.2 Nanofluid modeling

Thermo-physical and transport properties of nanofluids are very important in the study of nanofluid flow and thermal physics. So far, most studies on nanofluid thermal properties have focused on thermal conductivity and viscosity. However, two phase flow and heat transfer characteristics also depend on other properties, such as specific heat and density etc. In Eqs. (3.2) to (3.6), physical properties such as density  $\rho_{nf}$ , thermal expansion coefficient  $\beta_{nf}$  and viscosity  $\mu_{nf}$  of the nanofluid are defined in [13] as

$$\rho_{nf} = (1-\phi)\rho_f + \phi\rho_s, \quad (3.11)$$

$$(\beta)_{nf} = \frac{(1-\phi)(\rho\beta)_f + \phi(\rho\beta)_s}{\rho_{eff}}, \quad (3.12)$$

$$\mu_{nf} = \frac{\mu_f}{(1-\phi)^{2.5}}. \quad (3.13)$$

The effective thermal conductivity  $k_{nf,eff}$ , electric conductivity  $\sigma_{nf,eff}$  and heat capacitance  $(C_p)_{nf,eff}$  models are specified as follows

$$k_{nf,eff} = \frac{k_m k_{nf}}{\varepsilon k_m + (1-\varepsilon)k_{nf}}, \quad (3.14)$$

$$\sigma_{nf,eff} = \frac{\sigma_m \sigma_{nf}}{\varepsilon \sigma_m + (1-\varepsilon)\sigma_{nf}}, \quad (3.15)$$

$$(C_p)_{nf,eff} = \frac{(1-\varepsilon)(\rho C_p)_m + \varepsilon(\rho C_p)_{nf}}{\rho_{nf}}. \quad (3.16)$$

In above, the subscripts  $m$  and  $nf$  are used for packing beds nanofluid. In the present of nanoparticles,  $\sigma_{nf}$  is the electric conductivity,  $(C_p)_{nf}$  heat capacitance and thermal conductivity is given as

$$\sigma_{nf} = \frac{\sigma_s + 2\sigma_f + 2(\sigma_s - \sigma_f)\phi}{\sigma_s + 2\sigma_f - (\sigma_s - \sigma_f)\phi} \sigma_f, \quad (3.17)$$

$$(C_p)_{nf} = \frac{(1-\phi)(\rho C_p)_f + \phi(\rho C_p)_s}{\rho_{nf}}, \quad (3.18)$$

$$k_{nf} = \frac{k_{pc} + 2k_f + 2(k_{pc} - k_f)(1 + \beta^*)^3 \phi}{k_{pc} + 2k_f - (k_{pc} - k_f)(1 + \beta^*)^3 \phi} k_f. \quad (3.19)$$

Where thermal conductive  $k_{pc}$  with layer around the particles is defined by

TH-16772

$$k_{pe} = \frac{[2(1-\gamma) + (1+\beta^*)^3(1+2\gamma^*)]\gamma^*}{-(1-\gamma^*) + (1+\beta^*)^3(1+2\gamma^*)} k_s, \quad (3.20)$$

here  $\gamma^* = k_{layer} / k_s$  is the ratio of nanolayer and particle thermal conductivities.

### 3.3 Heat transfer coefficient

The most important result to be determined is the heat transfer rate from the vertical plate. To understand the convection boundary layers, it is necessary to understand convective heat transfer between a surface and a fluid flowing past it is usually presented in terms of the Nusselt number is given as

$$Nu_x = \frac{hx}{k_f}, \quad (3.21)$$

where

$$h = \frac{-k_{nf} \left. \frac{\partial(T - T_\infty)}{\partial y} \right|_{z=0}}{(T_w - T_\infty)}. \quad (3.22)$$

The local Nusselt number in terms of the new variable is

$$\frac{Nu_x}{Gr_x^{1/4}} = -\frac{k_{nf}}{k_f} \theta(0) \quad (3.23)$$

### 3.4 Solution of the problem

Due to nonlinear nature of Eqs. (3.9) and (3.10), an exact solution is not possible. Now, we opted to go for series solution. To this end, the Mathematica package BVPh 2.0 [12] which is based on the homotopy analysis method employed for solving nonlinear ordinary differential equation using computational software Mathematica 9. In this package, one has great freedom to choose the auxiliary linear operator and initial guess. To run the package, need to define all the inputs of problem properly, except the convergence-control parameters. In this package, it is needed to put appropriate initial guess of solutions and auxiliary linear operators to find the desire solution and are given as



$$\left. \begin{aligned} \xi_f &= \frac{d^3}{d\eta^3} - \frac{d}{d\eta}, \\ \xi_\theta &= \frac{d^2}{d\eta^2} - 1 \end{aligned} \right\} \quad (3.24)$$

$$\left. \begin{aligned} f_o(\eta) &= \frac{1}{2} + \frac{1}{2} e^{-2\eta} - e^{-\eta}, \\ \theta_o(\eta) &= e^{-\eta} \end{aligned} \right\} \quad (3.25)$$

Further, the results for velocity components and temperature up to first iteration are as follow:

$$\begin{aligned} f = & \left( \frac{1}{2} + \frac{37}{300} \frac{(\rho\beta)_{nf}}{(\rho\beta)_f} - \frac{37C}{3000} \frac{\rho_{nf}}{\rho_f} \right. \\ & \left. - \frac{37\Lambda}{600} \frac{\mu_{nf}}{\mu_f} - \frac{37}{300\varepsilon} \frac{\mu_{nf}}{\mu_f} - \frac{37M}{300\varepsilon} \frac{\sigma_{nf}}{\sigma_f} \right) + \left( -1 - \frac{37}{150} \frac{(\rho\beta)_{nf}}{(\rho\beta)_f} + \frac{37C}{1500} \frac{\rho_{nf}}{\rho_f} \right. \\ & \left. + \frac{37\Lambda}{240} \frac{\mu_{nf}}{\mu_f} + \frac{37}{300\varepsilon} \frac{\mu_{nf}}{\mu_f} + \frac{37M}{240\varepsilon} \frac{\sigma_{nf}}{\sigma_f} \right) e^{-\eta} \\ & \left( \frac{1}{2} + \frac{37}{600} \frac{(\rho\beta)_{nf}}{(\rho\beta)_f} - \frac{37M}{1200\varepsilon} \frac{\sigma_{nf}}{\sigma_f} \right) e^{-2\eta} + \left( -\frac{37C}{1200} \frac{\rho_{nf}}{\rho_f} + \frac{37\Lambda}{1200} \frac{\mu_{nf}}{\mu_f} \right) e^{-3\eta}, \\ & + \left( \frac{37C}{1500} \frac{\rho_{nf}}{\rho_f} \right) e^{-4\eta} - \left( \frac{37C}{6000} \frac{\rho_{nf}}{\rho_f} \right) e^{-5\eta} \end{aligned} \quad (3.26)$$

$$\begin{aligned} \theta = & \left( \frac{22}{75} \frac{k_{nf}}{k_f} - \frac{99 \text{Pr}}{2000} \frac{(\rho C_p)_{nf}}{(\rho C_p)_f} \right) e^{-\eta} + \left( -\frac{22}{75} \frac{k_{nf}}{k_f} - \frac{33 \text{Pr}}{400} \frac{(\rho C_p)_{nf}}{(\rho C_p)_f} \right) e^{-2\eta} \\ & \left( 1 - \frac{33n \text{Pr}}{2000} \frac{(\rho C_p)_{nf}}{(\rho C_p)_f} \right) e^{-3\eta} + \left( \frac{11n \text{Pr}}{300} \frac{(\rho C_p)_{nf}}{(\rho C_p)_f} \right) e^{-4\eta} \\ & - \left( \frac{33 \text{Pr}}{400} \frac{k_{nf}}{k_f} \right) e^{-3\eta} + \left( \frac{11 \text{Pr}}{500} \frac{(\rho C_p)_{nf}}{(\rho C_p)_f} + \frac{11n \text{Pr}}{1500} \right) e^{-4\eta}. \end{aligned} \quad (3.27)$$

### 3.5 Results and discussion

In this section, to understand the behavior of particle concentration and porosity on flow field and heat distribution; streamlines, heat lines as well as velocity and temperature fields are plotted graphically. For nanofluid, water as base fluid and aluminum oxides is used as nanomaterial. In addition, thermal conductivity around nanoparticles of nanolayer thickness of 1nm is utilized.

The effects of particle concentration on flow of mass and heat, stream lines and heat lines are plotted in Figs. 3.2 to 3.9. The explorations of certain parameters influences on velocities and temperature profiles are representing in Figs. 3.2 to 3.7. The results velocities profiles with particles concentrations effects are shown in Fig. 3.2. It is perceived that several velocity lines have been exposed in resultant of different nanoparticles concentrations. By different concentration, divergent collisions between neighboring particles in a fluid are happen that produced diverse velocity lines. It is noticed that when the nanoparticle concentration is enhanced, resistance between adjacent layers of moving fluid is enhanced which leads to fall down in velocity profiles. Therefore, nanofluid particles are not moved quality as compare to base fluid particles. Fig. 3.3 shows the effect of particle concentrations on temperature profile. It is seen that the temperature of nanofluid is enhanced by increasing nanoparticles concentration. This enhancement in temperature is due to improvement in large thermal conduction of nanofluid. The effects of porosity on velocity field are illustrated in Fig. 3.4. It is known that permeability of a medium is related to the porosity. The permeability shows ability of a porous material to allow fluids to pass through it. In consequence of porosity enhancement, permeability is amplified which leads to augmentation of fluid flow in supposed porous medium. Therefore, due to porosity enhancement, velocity field is increased. Fig. 3.5 demonstrates the influence of porosity parameter on temperature distribution. It is seen that temperature is declined by increasing of porosity parameter. The main reason in reduction of temperature is thermal conductivity decay in consequence of porosity influence. The effect of magnitude of magnetic field strength on velocity is investigated in Fig. 3.6. It shows the velocity is declined when magnetic field is applied. It is due to alignment of particles in field direction that product a resistance in fluid flow. The results of magnetic strength effect on temperature profile are displaced in Fig. 3.7. It is seen that magnetic field have not effective influence on temperature as same for velocity profile. Under critical view, it is seen that temperature is little bit increased. In Fig. 3.8(a) to 3.8(d), stream lines are plotted corresponding to

different particle concentration. It is seen that flow field decreases near the vertical wall as compare to far from the wall and stream lines are slightly pushed towards the wall when particle concentration is reduced. Moreover, with reduction of nanoparticle concentration, displacement between layers is slightly decreased. In this consequence, mass has to move quickly between the layers which rising the flow speed. Figs. 3.9(a) to 3.9(d) show the heat lines under different particle concentration. It is seen that heat lines are similar to stream lines because both velocity and thermal profiles are developed simultaneously and fluid field have a strong influence on the temperature distribution. When concentration is enhanced, heat lines are scattered enormously. In this consequence, heat is distributed quickly which lead to enhancement in convection heat transfer rate.

The numerical sets of values show the results for parameters on local Nusselt number. The physical interpretation of Nusselt number is the enhancement of heat transfer due to convection over conduction. The Nusselt number has paramount importance because it contains the heat transfer coefficient information. Indeed, one interpretation of Nusselts number is simply that of dimensionless heat transfer coefficient. The impact of particle volume fraction, magnetic strength and porosity on local Nusselt or dimensionless heat transfer coefficient is shown in table 3.1. In this table, it is observed that when nanoparticle volume fraction enhances, the heat transfer at wall increases. It is known that thermal conduction of fluid plays an important role in the heat transfer enhancement. When particle concentration is increased, the thermal conductivity is improved and in this consequence heat transfer rate is increased as shown in table 3.1. On the other hand, when porosity of medium is improved, heat transfer rate is decreased. Thermal conductivity of fluid is decreased in this consequence of porosity enhancement which also a cause in reduction in heat transfer rate. In aspect of magnetic, same behavior is noted as porosity but not much effective in heat transfer rate as porosity has influence.

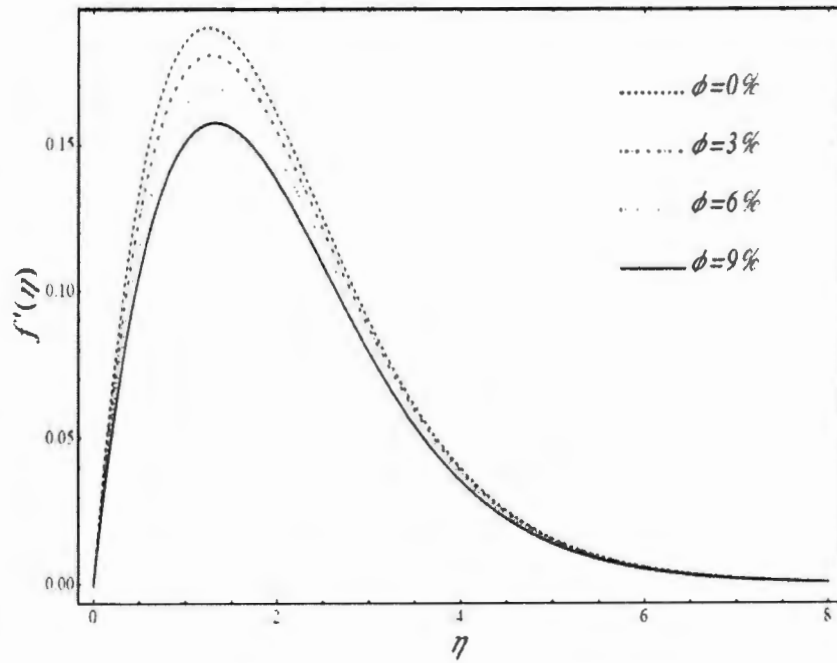


**Fig. 3.2.** Velocity profile corresponding to various nanoparticle concentrations when  $\varepsilon = 0.5$  and  $\beta_o = 0.3$ .

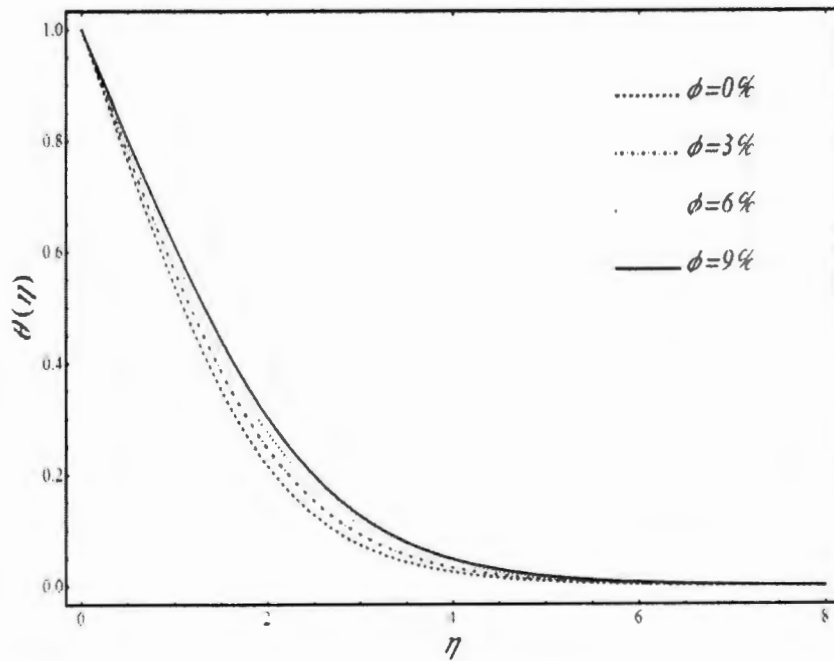


**Fig. 3.3.** Temperature profile corresponding to various nanoparticle concentrations when  $\varepsilon = 0.5$  and  $\beta_o = 0.3$ .

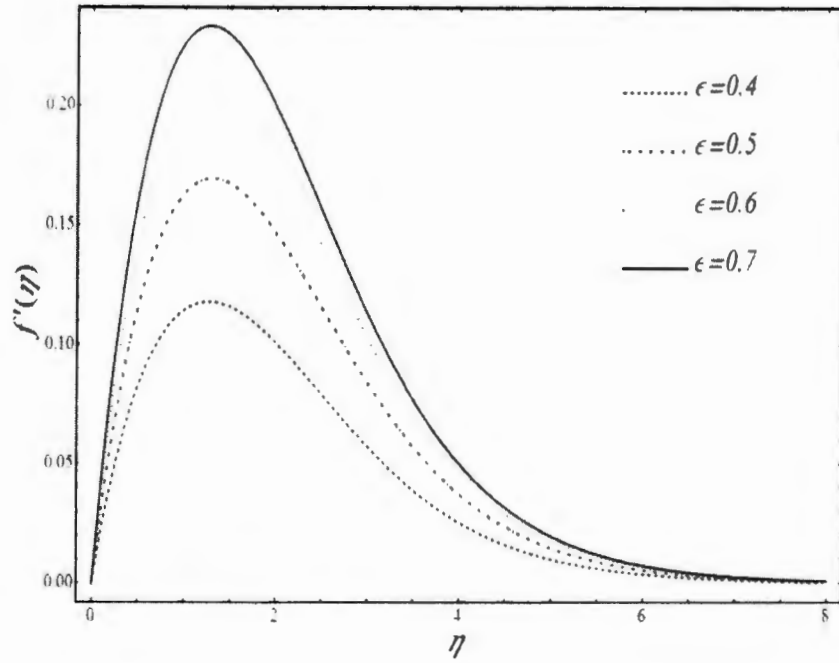


Fig. 3.4. Velocity profile corresponding to various values of porosity parameter when  $\phi = 3\%$  and  $\beta_o = 0.3$ .

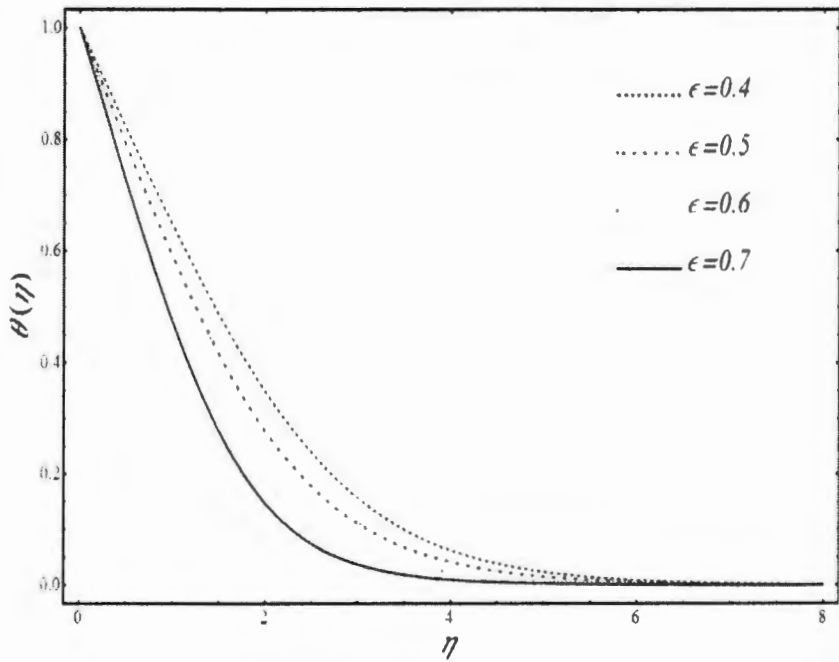
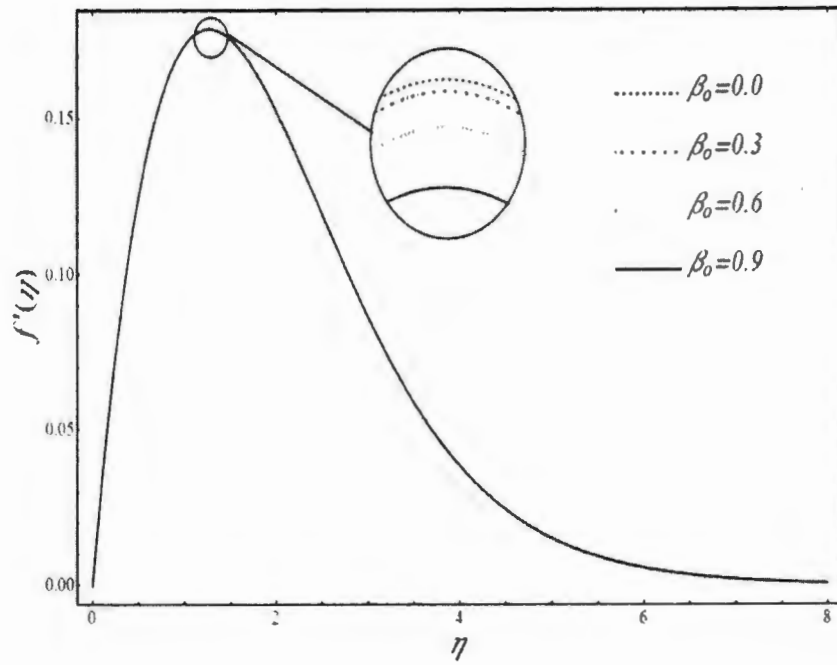
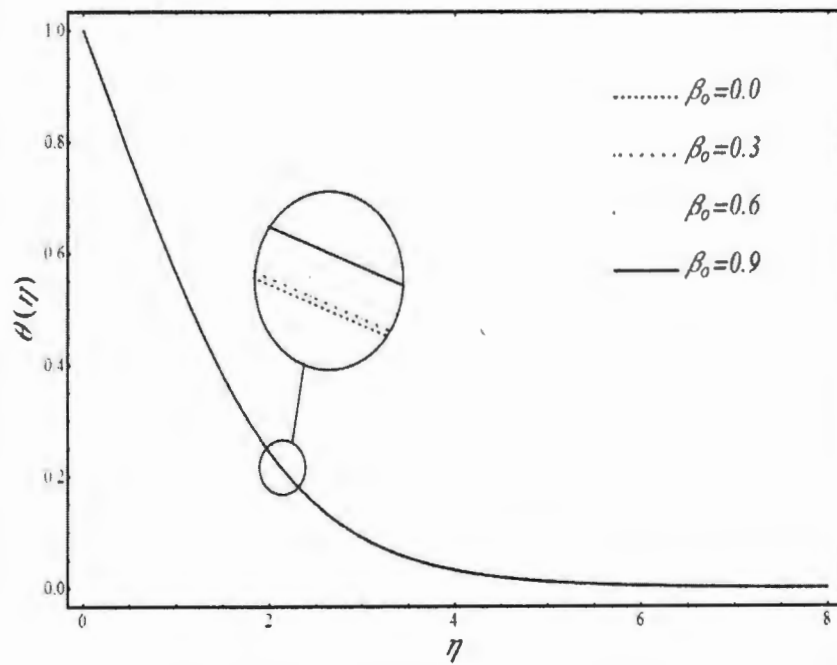


Fig. 3.5. Temperature profile corresponding to various values of porosity parameter when  $\phi = 3\%$  and  $\beta_o = 0.3$ .



**Fig. 3.6.** Velocity profile corresponding to various values of magnetic strength when  $\phi = 3\%$  and  $\varepsilon = 0.5$ .



**Fig. 3.7.** Temperature profile corresponding to various values of magnetic strength when  $\phi = 3\%$  and  $\varepsilon = 0.5$ .



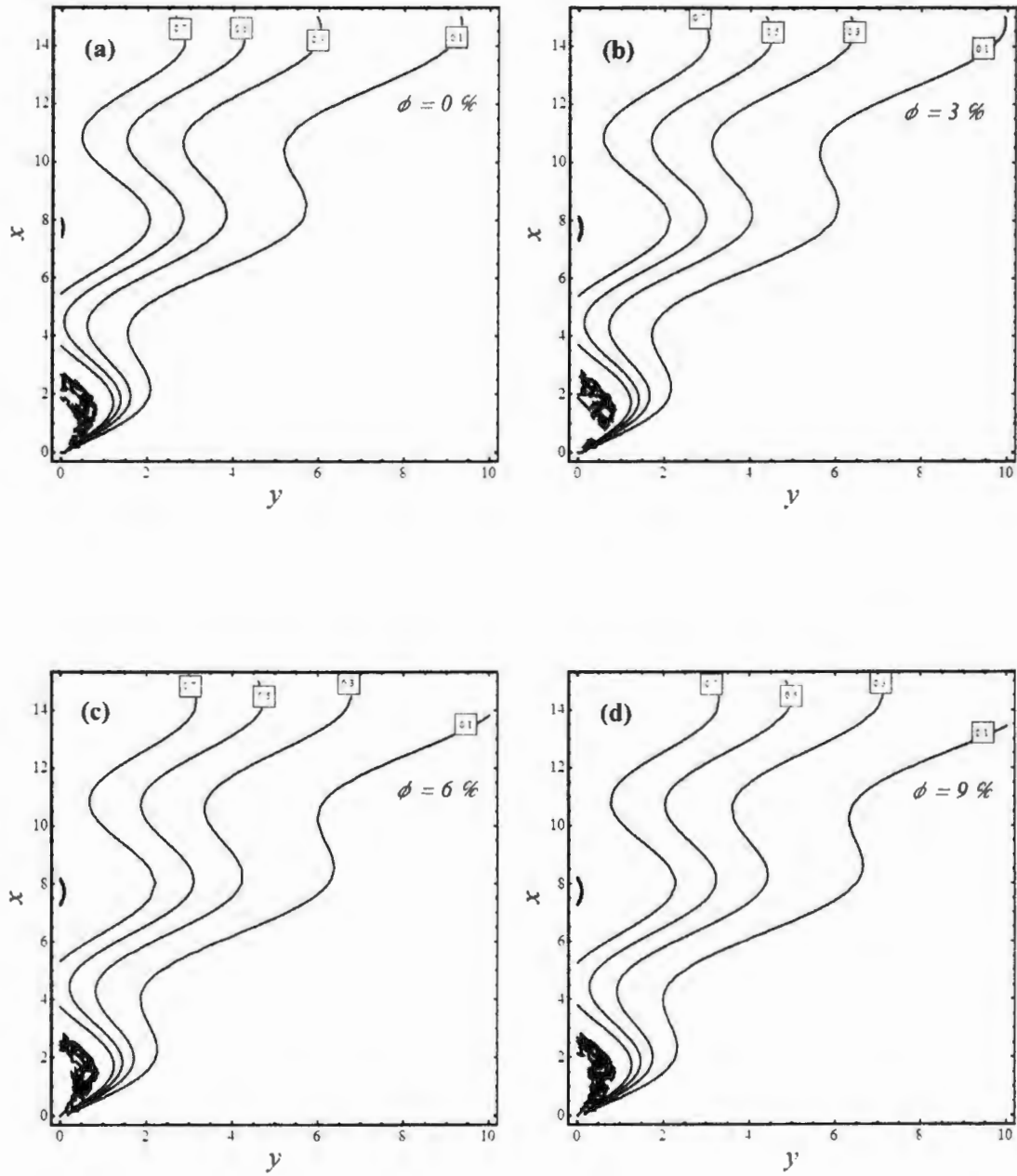


**Fig. 3.9.** Heatlines for (a) water and nanofluid at (b) 3% particle concentration, (c) 6% particle concentration and (d) 9% particle concentration when  $\varepsilon = 0.5$  and  $\beta_n = 0.3$ .



**Table. 3.1:** Values of skin-friction coefficient, local Nusselt, boundary layer thickness, volume flowing outward the z-axis and angle corresponding to various values of nanoparticle volume fraction.

$\phi$	$Nu$	$\varepsilon$	$Nu$	$\beta_o$	$Nu$
0%	20.8100	0.4	21.9411	0.0	21.3016
3%	21.3009	0.5	21.3009	0.3	21.3009
6%	21.8399	0.6	21.0178	0.6	21.2988
9%	22.4489	0.7	20.6645	0.9	21.2954

### 3.6 Concluding remarks

The present work examines heat transfer in non-Darcian flow phenomena over wavy surface. The main findings are listed as follows:

1. It is noted that by increasing the magnetic strength, velocity field and heat transfer rate decreases.
2. It is observed that flow speed increases by increasing the value of porosity parameter.
3. The convection heat transfer rate is reduced due to declination in thermal conduction in result of enhancement in porosity.
4. When nanoparticles are added in fluid, convection heat transfer rate is improved but these are affected to flow velocity.

## References

- [1] S. U. S. Choi, Developments and applications of non-Newtonian flows, ASME FED, 66 (1995) 99 – 105.
- [2] S. K. Das, S. U. S. Choi, W. Yu and T. Pradeep, Nanofluids Science and Technology, John Wiley, 2008.
- [3] H. Alfvén, Existence of electromagnetic – hydrodynamic waves, Nature, 150 (1942) 405 – 406.
- [4] M. Sheikholeslami, M. Gorji Bandpay and D. D. Ganji, Magnetic field effects on natural convection around a horizontal circular cylinder inside a square enclosure filled with nanofluid. Int. Commun. Heat Mass Transfer, 39 (2012) 978 – 986.
- [5] K. Vafai, Handbook of Porous Media, Taylor and Francis e-Library (2005).
- [6] D. Srinivasacharya, B. Mallikarjuna and R. Bhuvanavijay, Natural convection along a vertical wavy surface in a porous medium with variable properties and cross diffusion effects, International Journal of Nonlinear Science, 19 (2015) 53-64.
- [7] C. Y. Cheng. Natural convection heat and mass transfer near a vertical wavy surface with constant wall temperature and concentration in a porous medium. Int. Comm. Heat and Mass Transfer, 27 (2000) 1143–1154.
- [8] E. C. Lai and F. A. Kulacki. Effects of variable viscosity on convective heat transfer along a vertical surface in a saturated porous medium, International Journal of Heat and Mass Transfer, 33 (1990) 1189–1194.
- [9] M. S. Seddeek and A. M. Salem. Laminar mixed convection adjacent to vertical continuously stretching sheets with variable viscosity and variable thermal diffusivity, Heat and Mass Transfer, 41 (2005) 1048–1055.
- [10] J. C. Slattery. Momentum, Energy and Mass Transfer in Continua. Mc. Graw-Hill, New York, (1972).
- [11] A. A. Afify. Effects of variable viscosity on non-Darcy MHD free convection along a non-isothermal vertical surface in a thermally stratified porous medium, Applied Mathematical Modelling, 31 (2007) 1621-1634.
- [12] Y. Zhao and S. Liao. HAM-based package BVPh 2.0 for nonlinear boundary value problems, in S. Liao (Ed), Advance in Homotopy Analysis Method, Word Scientific Press, (2013).
- [13] M. Hassan. Study of convection flows in nanofluids, Phd thesis, Department of Mathematics and Statistics IIUI (2016).